Hindawi
Shock and Vibration
Volume 2018, Article ID 7018325, 24 pages
https://doi.org/10.1155/2018/7018325

Research Article

Investigation of Snow Load Effects on Modal Parameters of a Steel Structure Roof

Xiaoshu Guan[1], **Huipin Chen**[2], **Jian He**[1], **and Xiaodan Sun**[1]

[1]*College of Aerospace and Civil Engineering, Harbin Engineering University, Harbin 150001, China*
[2]*China Railway Construction Engineering Group Co., Ltd. Beijing Branch, China Railway Construction Engineering Group, Beijing 100160, China*

Correspondence should be addressed to Jian He; hejian@hrbeu.edu.cn

Received 19 April 2018; Revised 20 July 2018; Accepted 17 August 2018; Published 13 September 2018

Academic Editor: Emanuele Reccia

Snowfall is one of the environmental factors that can cause effects on the identification of structural modal parameters. For the steel structure roof of the Harbin Railway Station, effects of snow load to the modal parameters were investigated. A single-span simply supported beam was analysed from the theoretical perspective to study the principles. FEM-based analyses were conducted for the steel structure roof to illustrate the significance of the snow load effects to modal parameters. Uniformly and nonuniformly distributed snow loads were regarded as the essential factors influencing modal frequencies and mode shapes. Monitoring response data are collected and analysed to confirm the accuracy of analytical results. It is concluded that snowfall-induced variations on structural stiffness and mass matrices reduce the modal parameters and alter the mode shapes. The differences between the change regulations of the various modes are closely related to the distributions of snow loads. The theoretical and numerical analytical results are validated to be feasible and credible using temperature, axial strain, and acceleration measurements from the Harbin Railway Station field monitoring system.

1. Introduction

Over the past thirty years, damage identification has been focused on the structural health monitoring (SHM) field. Due to advances in sensor technology, integrated structural health monitoring system can be more widely used to improve the reliability, durability, longevity, system performance, and safety of a structure that could potentially be affected by natural disasters and accidental damage [1]. Furthermore, based on many proposed damage identification methods, the identification of modal parameters through vibration response data has been widely used in damage detection, development of early warning systems and safety assessments of actual structures. Nevertheless, environmental factors can deter the application of these methods, which can obstruct the identification of modal parameters and reduce the reliability of SHM. Specifically, environmental factors such as snow, wind, temperature, freeze, and thaw conditions alter the response of structures and thus impeding reliable damage identification. Therefore, it is of great interest to study the responses of structures under environmental factors and the mechanisms that cause these responses.

Study on responses of a long-span spatial structure caused by snowfall has always been a major research project and attracted worldwide attention from scientists in relevant fields. Snowfall can increase the structural burden, alter the dynamic response of the structure, and increase the difficulty of damage identification. In the 1990s, Majowiecki studied the design methods of long-span subhorizontal structures under snow loads through experimental analysis and noted that the most important factors were the drift and accumulation factors of the snow load. Additionally, the monitoring of actual structures was proposed by Majowiecki as a method of controlling the subsequent structural behaviour and improving design methods and theoretical analysis [2]. However, monitoring of actual structures is a long-term and complex work. Significant parameters associated with snow load, such as the total mass, thickness, density, viscosity, and distribution, usually differ based on the region and local weather patterns. Furthermore, the associated effects can

greatly vary based on the actual forms of structures. Therefore, it is difficult to develop a research method that can be applied to different types of structures.

As a significant environmental factor, snowfall often causes damage to long-span spatial structures. Therefore, the past main emphasis of the research is more concentrated in the load-bearing capacity and static responses of structures under snow loads. A large number of studies have extensively investigated the distribution of the snow load in different regions based on numerical and experimental methods. Originally, snow load was considered as the product of a ground load and a dimensionless ground-to-roof conversion factor. In 1985, Ellingwood and O'Rourke proposed probability models for ground snow accumulation and the ground-to-roof conversion factor [3]. Over time, additional factors of influence, such as wind, have been considered. By verifying previous research and analysing windward roof step data, O'Rourke and De Angelis justified the rationality of the consideration of windward drifting and verified the reliability of the proposed method [4]. Meløysund et al. suggested improvements to calculations of wind exposure for roof snow loads in Norway by determining exposure coefficients based on data from meteorological stations [5]. However, research on distributions cannot reflect the dissimilar responses caused by snow load to different structural types. Subsequently, analytical studies of snow load effects have been performed for certain structural types. Using the linear thin-shell theory of Sanders, Plaut et al. proposed an analytical solution for the initial stress on an arbitrary arch centerline structure under snow and wind loading [6]. Holicky and Sykora proposed a safety design procedure for lightweight steel roofs exposed to snow loads and calculated the 3 associated reliability indexes [7]. Additionally, based on the load-bearing capacity status and the failure on actual structures, a number of studies of the effects of snow loads on specific structures have been published and serve as references for related analysis methods. Lazzari et al. proposed nonlinear dynamic analysis methods considering the static and dynamic effects of wind and snow on the roof of Montreal Olympic Stadium to assess the associated structural behaviour [8]. Using a football stadium roof in Poland as an example, Flaga et al. obtained new similarity criteria numbers considering dispersion theory and factors such as snow precipitation and redistribution [9]. Additionally, del Coz Díaz et al. conducted a failure assessment based on sophisticated nonlinear finite element models to discuss the collapse of a self-weighted metallic roof [10]. Based on the Euler-Euler method in multiphase flow theory, Sun et al. presented a numerical simulation method combined with a snow deposition and erosion model to analyse the mechanical performance of a long-span membrane roof under a snowdrift [11].

As described above, for long-span spatial structures, studies of the responses under snow loads have mainly been performed from a static perspective. The distribution of snow loads and the load-bearing capacity of the structures under its action have been widely investigated. However, research regarding dynamic responses is not comprehensive. For the SHM area, using dynamic response data for modal parameter identification is of great significance. Modal parameters are often used as judging factors for damage identification and condition assessment of long-span spatial structures. Research on the changes of modal parameters caused by snow loads is helpful to the safety assessment of long-span spatial structures. Furthermore, studies on this topic can reduce the impact of snowfall and improve the accuracy and reliability of damage assessment based on SHM. Therefore, in this paper, effects of snow load on modal parameters of the steel structure roof from the Harbin Railway Station are analysed. The next section explains the principle of effects caused by snow loads on modal parameters. In Section 3, analytical investigations of the steel structure roof under uniformly and nonuniformly distributed snow loads are performed. The monitoring results are reported in Section 4, and the conclusions are summarized in Section 5.

2. Investigation on Principles of Snow Load Effects on Modal Parameters

Snowfall covers the roof of long-span spatial structures and transfers the load to structures. As a result, it not only influences the load-bearing capacity but also alters the stiffness matrix and mass matrix of the structure. However, due to the indeterminacy and temporal variations, it is complex and difficult to monitor the effects of snow load on modal parameters. Considering these reasons, it is difficult to develop snow load models in practice, even for specific structures. To investigate the relationships between snow load factors and modal parameters, a single-span simply supported beam was selected for analysis as a fundamental mechanical model.

The roofs of spatial structures are covered with uniformly or nonuniformly distributed snow loads. Because the snow load is not part of the structure, it is grouped with the roof panels in force analyses. When roof panels are continuously supported by structural members, the snow load, via the roof panels, can alter the force state on these members. For a single-span, continuous, equal cross-sectional beam with length l, modulus of elasticity E, second moment of area J, density ρ, and axial force T (a positive value represents a tensile force), the crosswise vibration equation can be expressed as follows [12, 13]:

$$EJ\frac{\partial^4 y}{\partial x^4} - T\frac{\partial^2 y}{\partial x^2} + \overline{m}\frac{\partial^2 y}{\partial t^2} = q, \tag{1}$$

where y is the transverse displacement over time t at position x along the span, $\overline{m}$ is the linear density, and q is the transverse distributed load. Without considering the effect of damping, the transverse vibration frequency of the n-th mode is given by the following equation [14]:

$$f_n = \frac{n\pi}{l}\sqrt{\frac{EJ}{\rho}\left(1 + \frac{Tl^2}{n^2\pi^2 EJ}\right)}. \tag{2}$$

According to Equation (2), assuming that the snow load is uniformly distributed, the relationship between the transverse vibration frequency f_n and density ρ can be expressed as $f_n \propto 1/\sqrt{\rho}$. In other words, the modal frequency decreases with increasing snow load, and the rate of reduction gradually decreases.

When the roof panels are supported by uniformly distributed junctions of the structure, it is more accurate to regard the snowfall as centralized masses at certain positions. Nevertheless, the positions and characteristics of each concentrated mass have different effects on the modal parameters of structures. Furthermore, concentrated masses at some specific positions can have distinct effects on certain modes [15]. In this case, a simple supported beam with one concentrated mass M can be used as an example. Based on Equation (1) and the boundary conditions for a simple supported beam, the transverse principal vibration equation of the n-th mode can be written as follows:

$$y_n(x,t) = A_n \sin\left(\frac{n\pi}{l}x\right) \cdot \sin(\omega_n t + \varphi_n), \tag{3}$$

where A_n is modal vibration amplitude of the n-th mode, ω_n is the circular frequency, and φ_n is the initial phase at time t. Assuming that the concentrated mass is located at the antisymmetric vibratory position of a certain mode, as shown in Figure 1, the boundary conditions can be represented as follows:

$$y_{\mathrm{n}}(b,t) = 0, \tag{4}$$

$$\frac{\partial^2 y_{\mathrm{n}}(b,t)}{\partial x^2} = 0. \tag{5}$$

Substituting Equation (4) and (5) into Equation (3) yields the following expressions:

$$A_n \sin\left(\frac{n\pi}{l}b\right) \cdot \sin(\omega_n t + \varphi_n) = 0, \tag{6}$$

$$-\frac{n^2\pi^2}{l^2}A_n \sin\left(\frac{n\pi}{l}b\right) \cdot \sin(\omega_n t + \varphi_n) = 0. \tag{7}$$

According to Equation (6) and Equation (7), $n\pi b/l = k\pi\,(k = 1, 2, 3\ldots)$. For a concentrated mass M, the inertial force of transverse motion provided by the simple supported beam can be formulated as follows:

$$\frac{1}{2}M\left[\frac{\partial^2 y(b,t)}{\partial t^2}\right]_{\max} = \left\{\frac{1}{2}M \cdot A_n \sin\left(\frac{n\pi}{l}b\right) \cdot \left(-\omega_n^2\right) \cdot \sin(\omega_n t + \varphi_n)\right\}_{\max} \equiv 0. \tag{8}$$

Equation (8) indicates that no transverse vibration occurs for concentrated mass M when arranged at the antisymmetric vibration positions of certain modes. In other words, the effect of the concentrated mass M does not influence this specific mode.

When one or several concentrated masses are arranged at ordinary positions along the simple supported beam, the associated calculations can be extremely complicated [16]. Therefore, a multiple-degree-of-freedom simplified model is developed to illustrate the inner relationships, as shown in Figure 2(a).

In this study, the first seven modal frequencies and mode shapes of the simplified models are calculated using the subspace iteration method. For an undamped transverse vibration system with multiple degrees of freedom, the vibration equation can be represented as follows [17]:

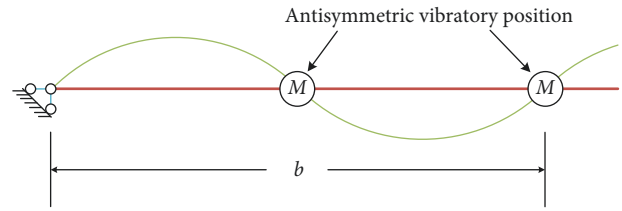

Figure 1: Transverse antisymmetric vibration of the simple supported beam.

$$\mathbf{M}\ddot{x} + \mathbf{K}x = 0, \tag{9}$$

where $\mathbf{M}$ and $\mathbf{K}$ are the mass and the stiffness matrices of the system, respectively. For the simplified model shown in Figure 2(a), the mass matrix $\mathbf{M}$ can be represented as follows:

$$\mathbf{M} = \frac{m_{\mathrm{L}}}{8}\begin{bmatrix} 1&0&0&0&0&0&0\\ 0&1&0&0&0&0&0\\ 0&0&1&0&0&0&0\\ 0&0&0&1&0&0&0\\ 0&0&0&0&1&0&0\\ 0&0&0&0&0&1&0\\ 0&0&0&0&0&0&1 \end{bmatrix}, \tag{10}$$

where m_{L} represents the total mass of the simplified model. For a multiple-degree-of-freedom system, the flexibility matrix $\boldsymbol{\delta}$ is the inverse matrix of the stiffness matrix $\mathbf{K}$, which can be represented as follows:

$$\mathbf{K}^{-1} = \boldsymbol{\delta} = \frac{l^3}{12288EJ}\begin{bmatrix} 49&81&95&94&81&59&31\\ 81&144&175&176&153&112&59\\ 95&175&225&234&207&153&81\\ 94&176&234&256&234&176&94\\ 81&153&207&234&225&175&95\\ 59&112&153&176&175&144&81\\ 31&59&81&94&95&81&49 \end{bmatrix}, \tag{11}$$

where l is the length, E is the modulus of elasticity, and J is the second moment of the area of the simplified model. Based on the subspace iteration method, the calculation results of first seven mode shapes without concentrated masses are shown in Figure 3.

As shown in Figure 2(b), the modal parameters of the simplified model with a single concentrated mass are investigated. The concentrated mass M varies within a range of

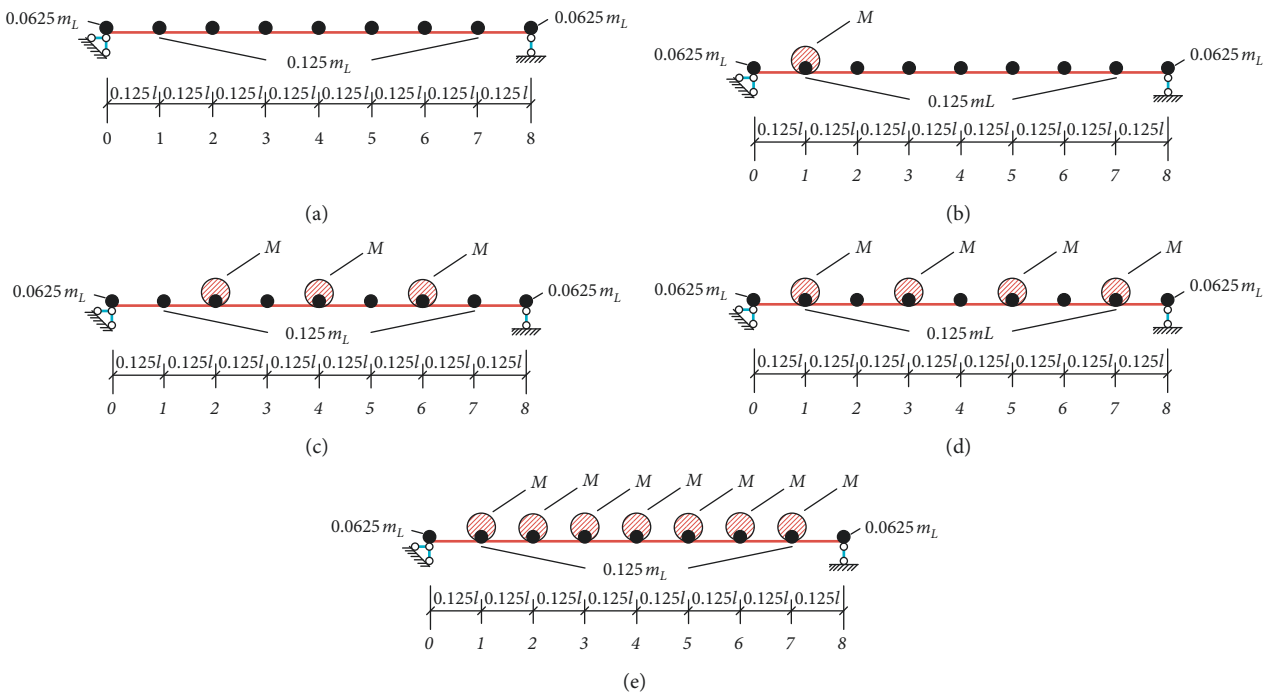

Figure 2: The simplified model: (a) preliminary model; (b) model with 1 concentrated mass; (c) model with 3 concentrated masses; (d) model with 4 concentrated masses; and (e) model with 7 concentrated masses.

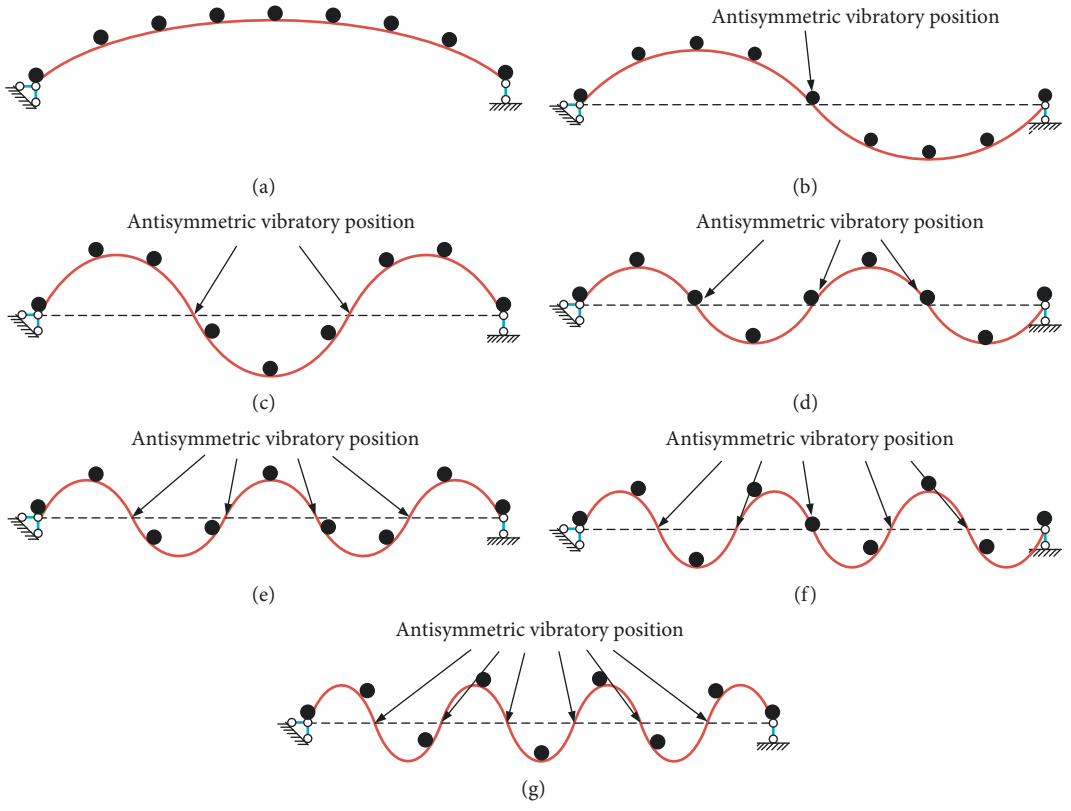

Figure 3: The first seven mode shapes of the simplified model: (a) the 1st mode; (b) the 2nd mode; (c) the 3rd mode; (d) the 4th mode; (e) the 5th mode; (f) the 6th mode; and (g) the 7th mode.

$0.0125\,m_L$ to $0.125\,m_L$. Considering the symmetry of the simplified model, the concentrated mass is considered at positions 1 to 4. The variations in the first seven modal frequencies are shown in Figure 4. The mode shape variations corresponding to the orders with significant and insignificant changes on frequencies are shown in Figure 5. The modal frequencies decrease as the concentrated mass increase, and the rate of decline progressively slows. Notably, this result is consistent with that for a continuously additional mass, as shown above. Variations in different modal frequencies differ as the position of the concentrated mass changes. As discussed above, locating the concentrated mass near the antisymmetric vibratory position of a certain mode causes little change in modal parameters. Conversely, when the concentrated mass is arranged at the high-amplitude positions of certain modes, the associated effects are larger. These results are supported by the calculations, taking the 4th and 7th modes as examples. Based on the mode shapes shown in Figure 3, position 1 is the position with the highest amplitude for the 4th mode and locates near the antisymmetric vibratory position for the 7th mode. Thus, the 4th modal frequency visibly changes along with the increasing concentrated mass, whereas the 7th modal frequency changes insignificantly. Correspondingly, an equivalent phenomenon can be observed for the mode shapes shown in Figure 5(a). Comparing these two mode shapes, that of the 4th mode changes more than that of the 7th mode. Additionally, changing the position of the concentrated mass also has analogous effects on certain modes. Figures 5(b)–5(d) show the most and least significant changes in the mode shapes when the concentrated mass is arranged at positions 2, 3, and 4. And the similar changing trends can also be observed for the corresponding modal frequencies, as shown in Figures 4(b)–4(d). These results indicate that the different changes among different modes are largely based on the distribution of the concentrated mass.

To illustrate the effects of multiple concentrated masses, simplified models with several concentrated masses are analysed, as is shown in Figures 2(c)–2(e). The first seven modal frequencies of the simplified models with three, four, and seven concentrated masses are shown in Figure 6. The mode shape variations corresponding to the orders with significant and insignificant changes on frequencies are shown in Figure 7. Although the total mass of the simplified model is increased, the difference caused by concentrated masses among the positions decreases. Thus, diversities of variations among the first seven frequencies are less obvious. In other words, the effects caused by the distribution of the concentrated mass gradually become weak, and it can be proved by the calculation results shown in Figure 6. The changes in the modal frequency are more and more similar to those caused by changing density, as discussed above. This result reflects the mutual agreement between these two theoretical analysis methods. Furthermore, a corresponding phenomenon can be observed for variations in mode shapes. For instance, although the 3rd modal frequency showed the most significant change, the 3rd mode shape did not show quite obvious variation, as shown in Figure 7(a). For the 4th mode, the three concentrated masses are arranged at antisymmetric vibratory positions. So the mode shape is virtually unchanged. For the simplified model with arranged concentrated masses on every multiple-degree-of-freedom, the varying modal frequencies overlap, as shown in Figure 6. It shows no diversities in the change regulation of modal frequencies among different modes. In this case, the effects caused by the distribution of concentrated masses no longer exist, i.e., the effects on modal parameters can be regarded as density variations and have no effect on mode shape, as illustrated by the 7th mode shape in Figure 7(c). In addition, when four concentrated masses are distributed, the 4th mode shape of the simplified model remains unchanged despite the significant variation in the modal frequency, as shown in Figure 7(b). For the 4th mode, the three positions without concentrated masses are the antisymmetric vibratory positions. Thus, the effects of the four concentrated masses on the 4th mode equate to the effects of seven concentrated masses. This result is supported by the similar variations of 4th modal frequencies in Figure 6(b)–6(c). It can be inferred that the degree of change in modal parameters is closely related to the differences among the positions caused by additional concentrated masses.

When regarding the snowfall as changing density of the simplified model or additional concentrated masses, the investigation results all show that the modal frequencies decrease at a decreasing rate along with increasing snow loads. Moreover, it can be deduced that changes of mode shapes are closely related to the distribution of snow load and the degree of change in the mass and stiffness matrices of the structure caused by the snow load. It should be noted that in this section, a simplified model with 7 degrees of freedom is created for simplicity. In reality, the number of degrees of freedom can be increased for further verification. Additionally, the damping ratio is a factor that is as important as the frequency and mode shape. However, to simplify the analysis process, it is not included in this study.

3. Analysis of Snow Load Effects on the Steel Structure Roof of Harbin Railway Station

3.1. Descriptions of the Structure and the Local Climate. The Harbin Railway Station is built in Harbin, Heilongjiang Province, which is known as one of the largest transportation hubs in Northeast China. An overall perspective of the railway station is shown in Figure 8. The roof of the train elevated station is constructed using a steel structure roof with dimensions of $162.15\,\text{m} \times 72\,\text{m} \times 13.25\,\text{m}$. The construction of the steel structure roof is divided into two phases and the completed first phase structure has dimensions of $69.75\,\text{m} \times 72\,\text{m} \times 13.25\,\text{m}$.

The steel structure roof is composed of transverse principal trusses and transverse secondary trusses arranged along the longitudinal direction, and these transverse trusses are together connected through longitudinal trusses. The completed first phase structure consists of 10 transverse arch trusses and 4 longitudinal vertical trusses, as is shown in Figure 9(a)–9(c). According to Figure 9(d), the trusses are composed of top chords, bottom chords and web members, which all constructed by steel pipes. The web members connect the top chords and the bottom chords to form the arched transverse trusses and the straight longitudinal

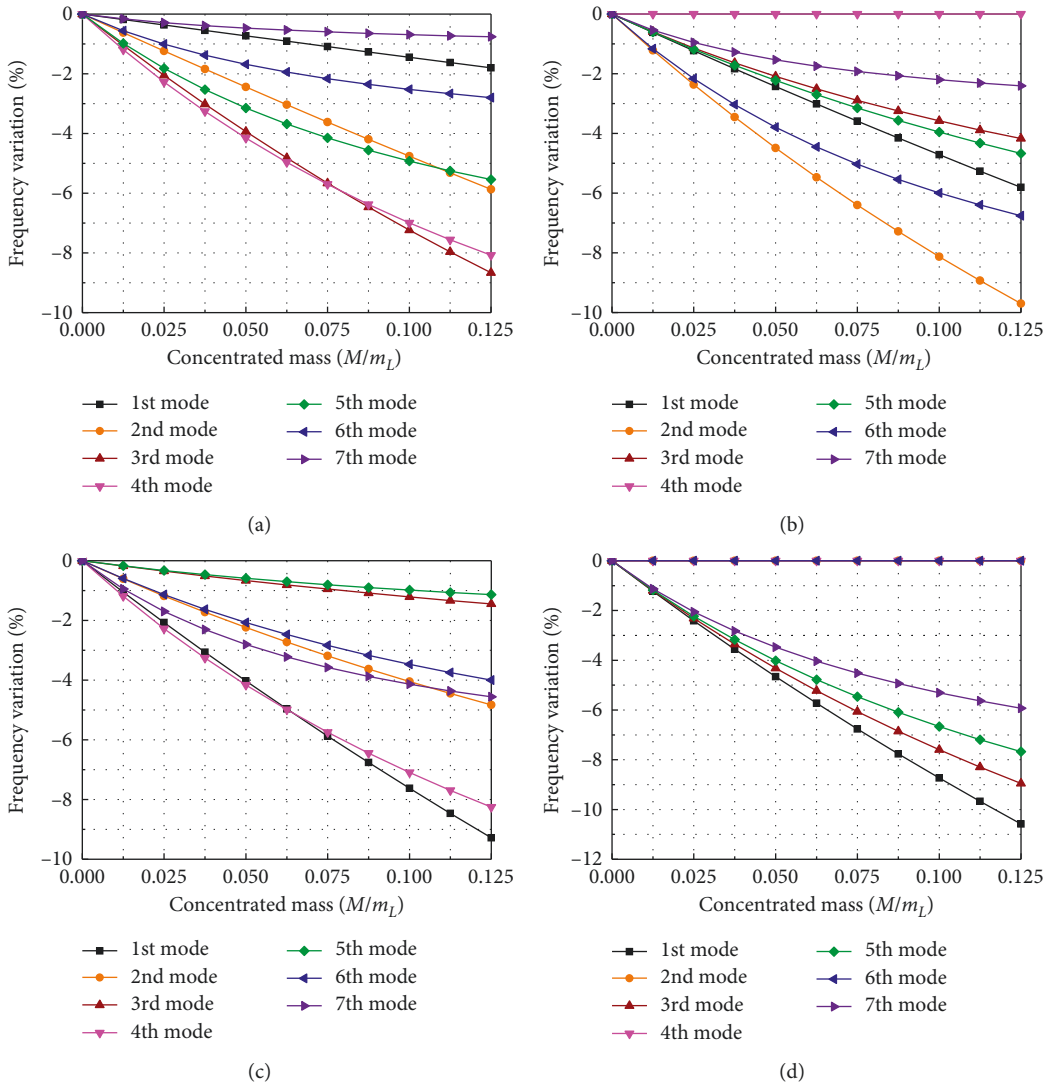

Figure 4: Frequency variations of the simplified model with 1 additional concentrated mass: (a) 1 concentrated mass on position 1; (b) 1 concentrated mass on position 2; (c) 1 concentrated mass on position 3; and (d) 1 concentrated mass on position 4.

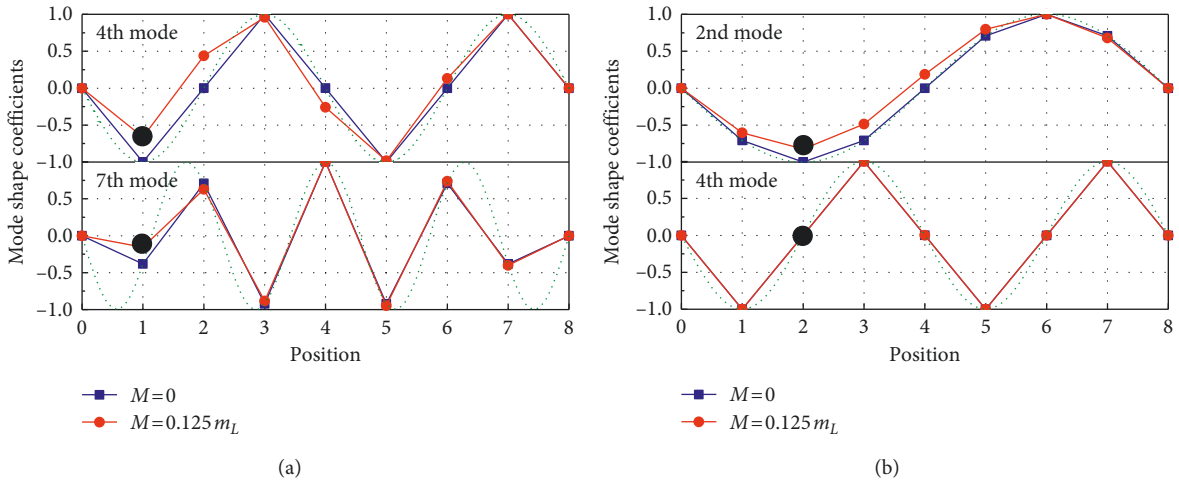

Figure 5: Continued.

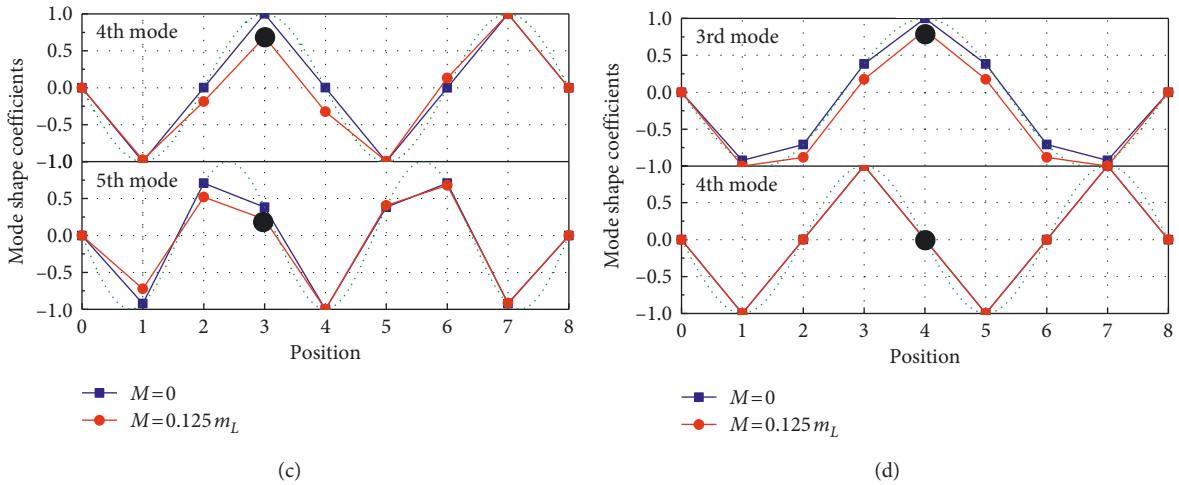

FIGURE 5: Mode shape variations of the simplified model with 1 additional concentrated mass: (a) 1 concentrated mass on position 1; (b) 1 concentrated mass on position 2; (c) 1 concentrated mass on position 3; and (d) 1 concentrated mass on position 4.

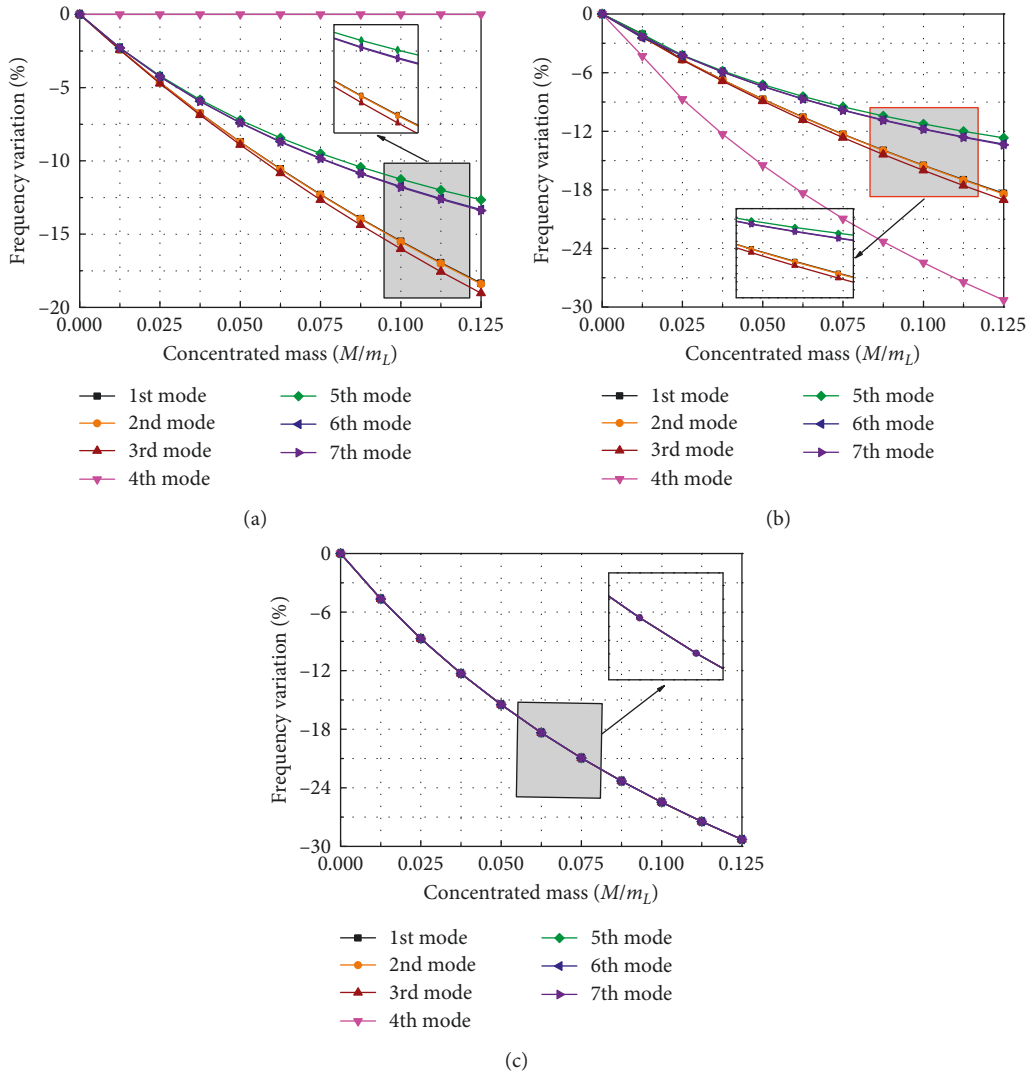

FIGURE 6: Frequency variations of the simplified model with several additional concentrated masses: (a) 3 concentrated masses on position 2, 4, and 6; (b) 4 concentrated masses on position 1, 3, 5, and 7; and (c) 7 concentrated masses on every position.

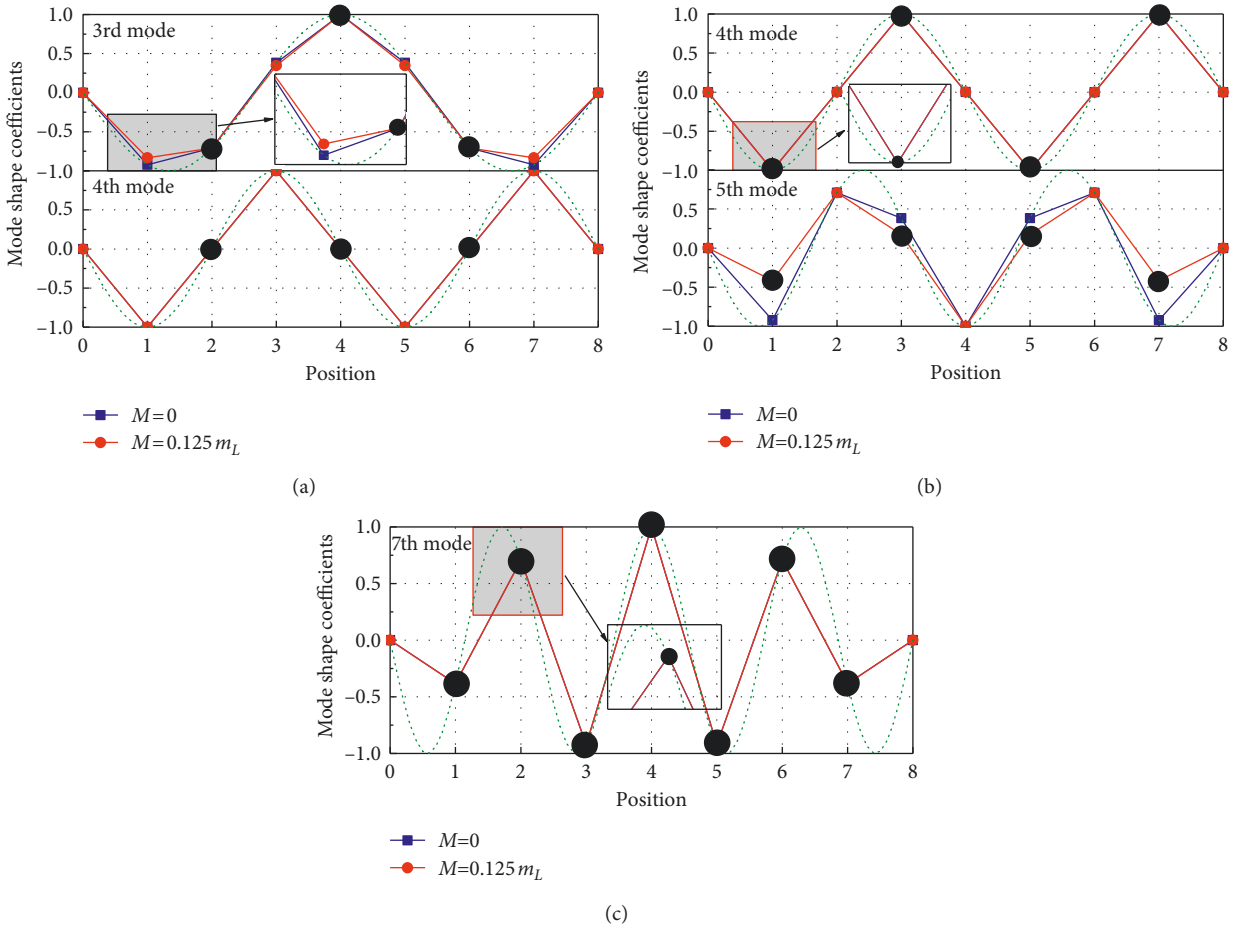

Figure 7: Mode shape variations of the simplified model with several additional concentrated masses: (a) 3 concentrated masses on position 2, 4, and 6; (b) 4 concentrated masses on position 1, 3, 5, and 7; and (c) 7 concentrated masses on every position.

Figure 8: Harbin railway station.

trusses. The whole structure is mounted on the concrete structure of the lower part through horizontal elastic supports and vertical rigid supports.

As a metropolis in northeastern China, Harbin has an annual temperature difference at around 70°C. The temperature can be as low as −35°C in winter. As mentioned above, environmental factors such as snowfall, wind, temperature, freeze, and thaw conditions alter the response of structures and change the modal parameters. In reality, wind is slight at Harbin and the effects to the Harbin Railway Station can be ignored. Additionally, according to the temperature variations of the steel structure roof shown in Figure 10, the maximum temperature difference from 1 Sep. 2017 to 31 Dec. 2017 is less than 10°C and the diurnal

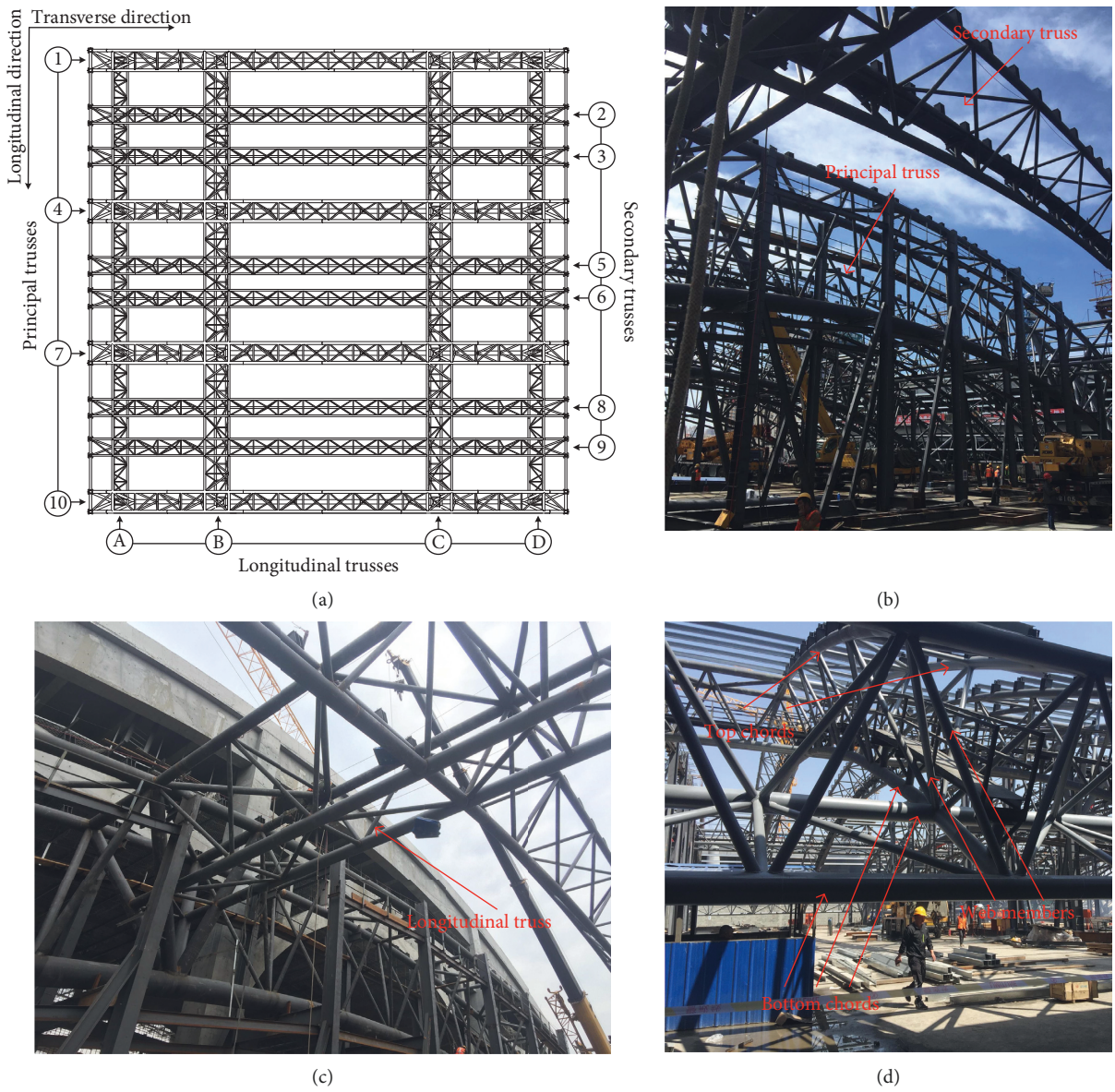

Figure 9: The completed first phase of the steel structure roof: (a) the arrangement of transverse trusses and longitudinal trusses; (b) the transverse trusses; (c) the longitudinal truss; and (d) the top chords, bottom chords, and web members.

temperature difference is less than 2°C. The temperature difference between the top and bottom chords is less than 1°C. Due to such insignificant temperature variations, it can be illustrated that the steel structure roof is almost unaffected by the ambient temperature. Therefore, the snowfall becomes the main factor for alterations of modal parameters.

3.2. FEM Analysis of the Structure. For the completed first phase of the steel structure roof, the FEM model was established through ANSYS, as shown in Figure 11. As a three-dimensional beam element, beam-188 element is suitable for analysing slender to moderately stubby or thick beam structures. Accordingly, 190,098 beam-188 elements were established to simulate all of the top chords, bottom chords, and web members of the structure. The combin-14 element contains the longitudinal spring-damper option and the torsional spring-damper option, which can provide longitudinal or torsional capability, respectively. So, 120 combin-14 elements were established to simulate the elastic supports. For the nonstressed components such as suspended ceilings and roof panels, they transfer their own loads to the steel structure roof. Because they are supported by uniformly distributed junctions on the top and bottom chords, it is more reasonable to consider them as additional concentrated masses. For mass-21 element, it can assign a different mass and rotary inertia to each coordinate direction. Therefore, all of the nonstressed components are simulated as centralized masses through 1830 mass-21 elements.

Due to the insignificant effects caused by wind and temperature to the steel structure roof, only the constant load of the structure and the nonstressed components are

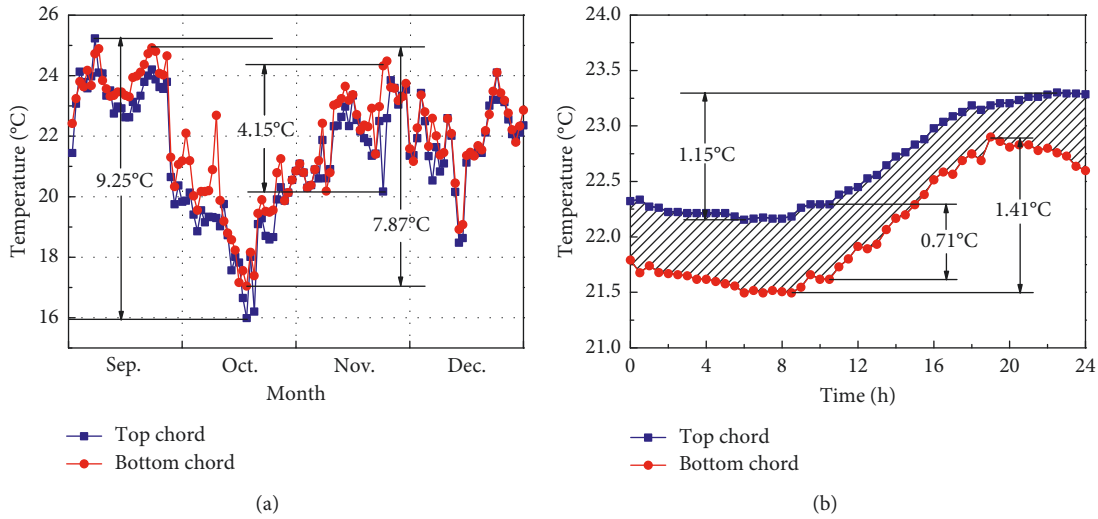

Figure 10: Temperature variation: (a) temperature variation from 1 Sep. 2017 to 31 Dec. 2017 at 12:00; and (b) temperature variation from 0:00 6 Nov. 2017 to 0:00 7 Nov. 2017.

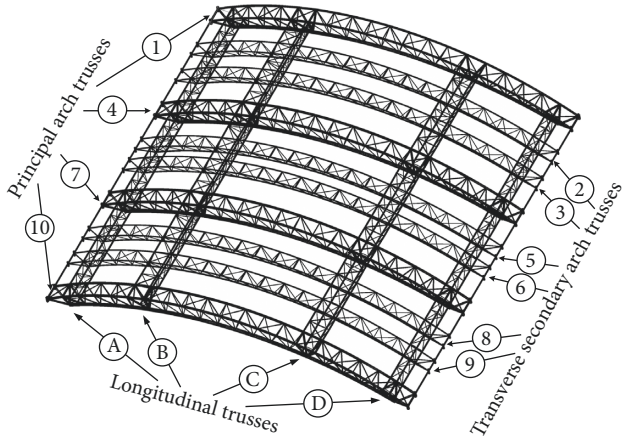

Figure 11: Overall FEM of the structure.

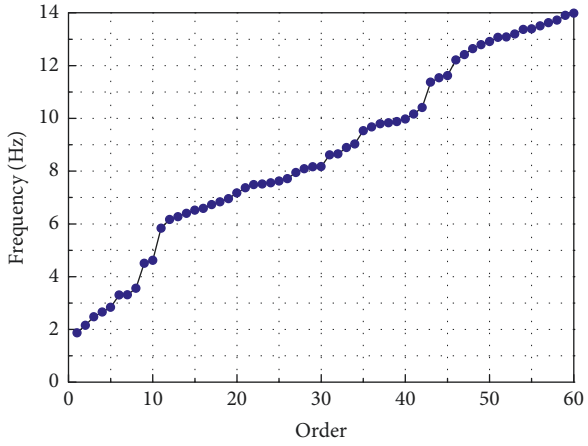

Figure 12: The first sixty frequencies.

considered. Without consideration of the snow load, the calculation results of the first 60 modes of modal frequency using the FEM at the reference ambient temperature (20°C) are shown in Figure 12. As a complex spatial structure, every degree of freedom of the steel structure roof has approximately identical mass and stiffness. Thus, the structure has closely spaced natural frequencies. Additionally, due to the actual form of the structure, stiffness and mass matrices on transverse, longitudinal, and vertical directions are quite different. Therefore, according to the first six mode shapes shown in Figures 13–18, distinctions on the stiffness and mass matrices make the three directions become the main vibration directions. The X, Y, and Z axes, respectively, represent the transverse, longitudinal, and vertical directions. The calculated modal frequencies and mass participation factors (MPF) for the first 6 modes are shown in Table 1. For the 1st mode with a mode shape of longitudinal vibration, the MPF has fairly large value on y direction (longitudinal). Additionally, as a mode of transverse vibration, the MPF values of the 2nd, 3rd, and 6th modes on x

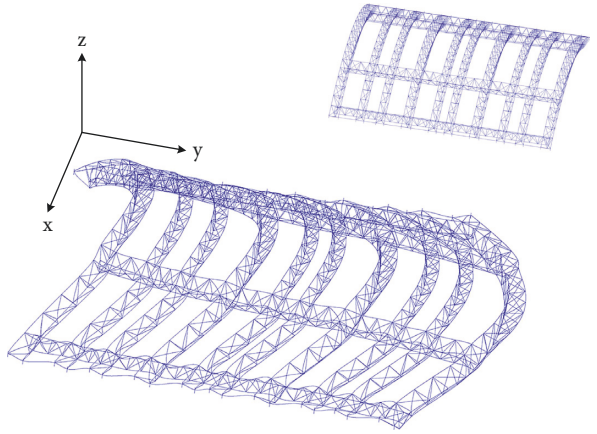

Figure 13: The 1st mode shape (longitudinal).

direction are larger as well. Similarly, the MPF values of 4th and 5th modes also have larger values on z direction because they are vertical vibrations. The correspondence between

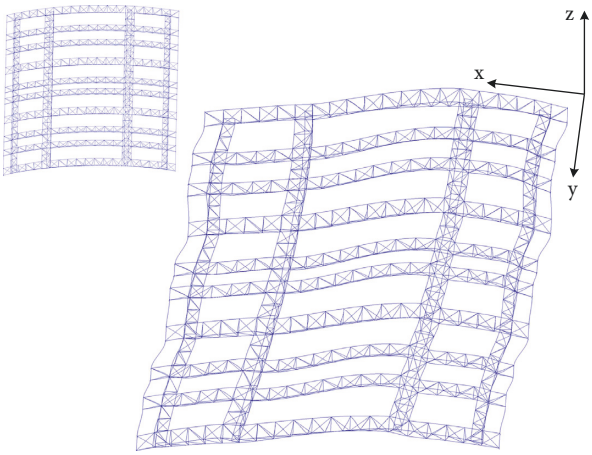

Figure 14: The 2nd mode shape (transverse).

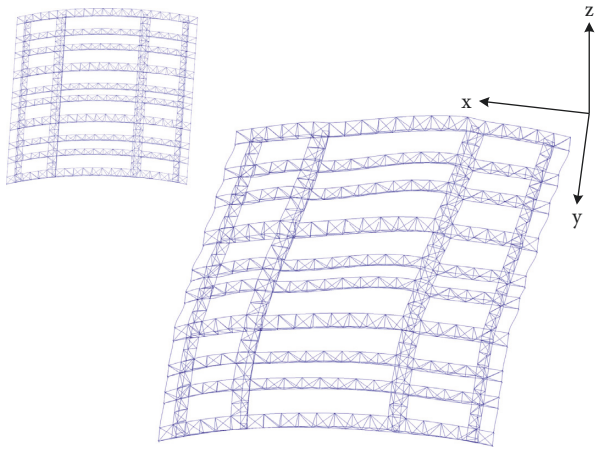

Figure 15: The 3rd mode shape (transverse).

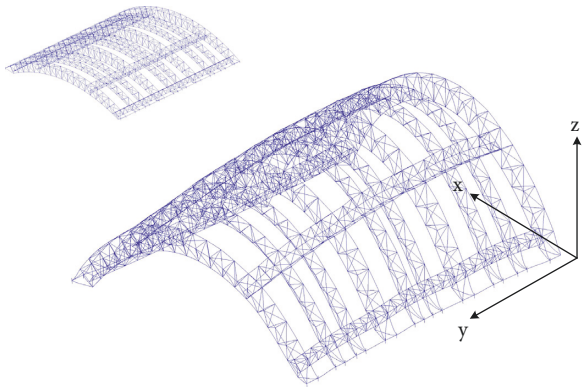

Figure 16: The 4th mode shape (vertical).

mode shapes and the MPF values reflects the accuracy of the calculation results.

3.2.1. Analysis of a Uniform Snow Load Distribution Condition. In this subsection, finite element model (FEM), static and dynamic analyses of the structural elastic stage

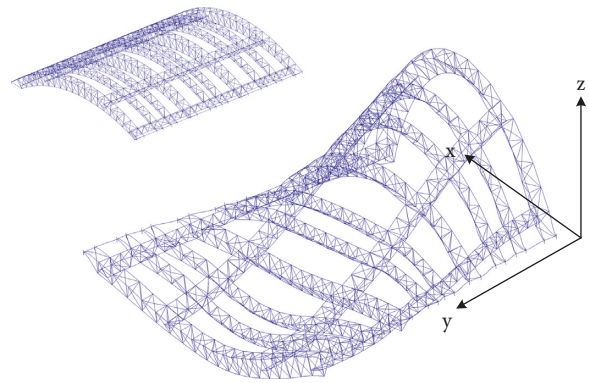

Figure 17: The 5th mode shape (vertical).

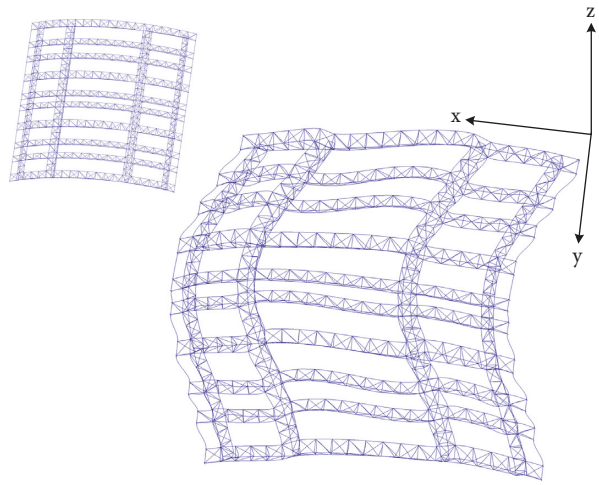

Figure 18: The 6th mode shape (transverse).

Table 1: The mass participation factors of the first 6 modes.

Modes	Frequency (Hz)	MPF (x direction)	MPF (y direction)	MPF (z direction)
1	1.868	$5.7502e-7$	0.088211	$2.9071e-3$
2	2.1515	0.13824	$2.0175e-05$	$9.2569e-6$
3	2.4782	0.043337	$1.3335e-05$	$1.1031e-5$
4	2.6548	$1.3547e-5$	0.051783	0.15724
5	2.8389	$1.7101e-6$	0.033359	0.043044
6	3.301	0.033303	$4.0892e-05$	$1.2661e-3$

were conducted. According to the discussion above, it can be determined that the snowfall is the only environmental factor with significant influence to the steel structure roof. Consequently, in addition to the constant load of the structure, only the effects of snow load on the first six modal parameters are considered. The other influential factors, such as the foundation, wind, and ambient temperature, are assumed to be invariable due to their insignificant effects.

Based on the load transfer mode of the steel structure roof, the weights of roof panels and snowfall are transferred to the roof through purlins. The purlins are fixed at certain locations on the top chords, as shown in Figure 19. So, the snowfall is considered as multiple concentrated masses.

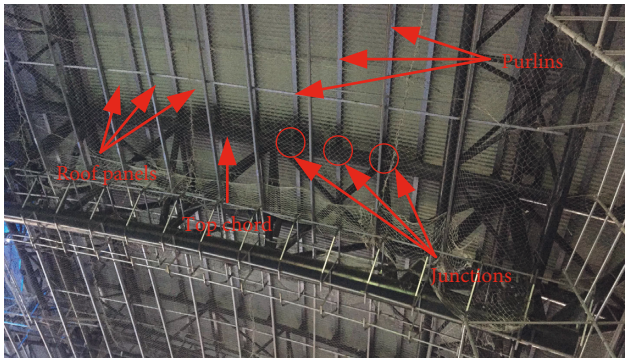

Figure 19: Steel structure roof.

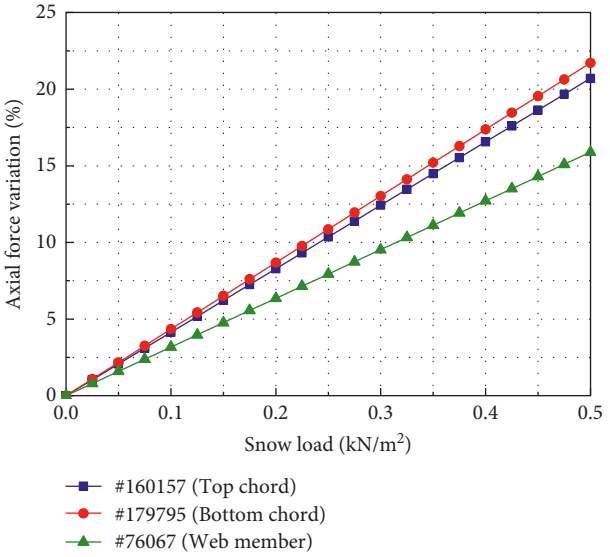

Figure 20: Axial force variation under uniformly distributed snow load.

It is assumed that the snowfall is uniformly distributed on the roof panels. Based on the reference of GB50009-2012 (*Load Code for the Design of Building Structures*) [18], the ground snow loads in Harbin with a return period of 100 years is 0.5 kN/m^2. So, in FEM of the steel structure roof, the snow load varies from 0 kN/m^2 to 0.5 kN/m^2, with an interval of 0.025 kN/m^2. The total mass of the snow load is equivalent to 22.1% of the structure weight. Because neither roof panels nor the snow is a force member, it is feasible and reasonable to treat them as additional concentrated masses.

As the snow load is varied, the structural internal forces are redistributed and can be reflected through axial force. Figure 20 shows the curves of axial force variations for three typical elements around the span center with a snow load (element 160157 and 179795 are top and bottom chords, respectively, and element 76067 is a web member, as is shown in Figure 21). The figure illustrates a linear relationship between the variations in the axial force and the snow load, which suggests that structural internal forces consistently increase along with the increasing snow load. Additionally, as the snow load is directly transferred to the top chords, the element on top chord exhibit the most significant change. Notably, changes in the axial force all vary by approximately 20%, as shown in Figure 20, because the total mass of the snow load is equivalent to 22.1% of the structure weight. Consequently, these results suggest that the change of stress status of the steel structure roof shows positive proportional relationship with the increments of snow load.

As a complicated space truss, the modal parameters of the steel structure roof are largely influenced by the actual form of the structure. Figure 22 shows negative relationships between the first six modal frequencies and the snow load. As discussed above, along with the increase in number of concentrated masses, the effects of the masses on the modal frequencies are similar to density changes. Due to the dense and uniform distribution of purlins shown in Figure 19, the snow load can be considered as a change in the density of top chords, as supported by the similar change trends in the modal frequencies illustrated in Figure 22. Because of the diversity in the stiffness and mass matrices in different directions, changes in certain modal frequencies caused by snow load differ. As a result, the 1st, 4th, and 5th modal frequencies exhibit relatively small reductions compared to those of the 2nd, 3rd, and 6th modes. For the first mode, which exhibits the most insignificant change in modal frequency, the mode shape shown in Figure 13 is a longitudinal vibration. The studied steel structure roof has the largest span in the longitudinal direction, and the integrity of the structure is strengthened by four longitudinal trusses. Thus, due to the high structural stiffness, the effects of the snow load are insignificant and do no visibly influence to the 1st modal frequency. Additionally, the steel structure roof has a fairly high stiffness in the direction of gravity. Therefore, because the 4th and 5th modes are vertical vibrations, the effects of the snow load on the associated modal frequencies are not obvious. By contrast, the transverse stiffness of the structure is mainly supplied by the four longitudinal trusses. Consequently, this structure has a comparatively low stiffness in the transverse direction. Therefore, modal frequencies of the 2nd, 3rd, and 6th modes exhibit significant variations in their transverse vibrations. Additionally, the 2nd and 3rd modes have similar mode shapes because the roof panels on the 10th truss were not installed for the convenience of further construction. Thus, the snow load is not applied to these panels, which results in differences between the mass matrix of the 10th truss and those of other trusses. Therefore, due to the local mass differences on the 10th truss, two modes with similar mode shapes and modal frequencies were produced. As discussed above, the degree of stiffness and mass variations caused by snow load is an important factor that influences variations in modal frequencies.

Additionally, mode shapes are important modal parameters that should be investigated. To quantify the variations in mode shapes, the Modal Assurance Criterion (MAC) is used as an index to evaluate the changes in mode shapes. The MAC can be defined as follows [19]:

$$\mathrm{MAC}\left(\varphi_i, \varphi_j\right) = \frac{\left(\varphi_i, \varphi_j^T\right)^2}{\left(\varphi_i, \varphi_i^T\right) \cdot \left(\varphi_j, \varphi_j^T\right)}, \tag{12}$$

where φ_i and φ_j are the mode shapes of modes i and j, respectively. The MAC values in three different directions are

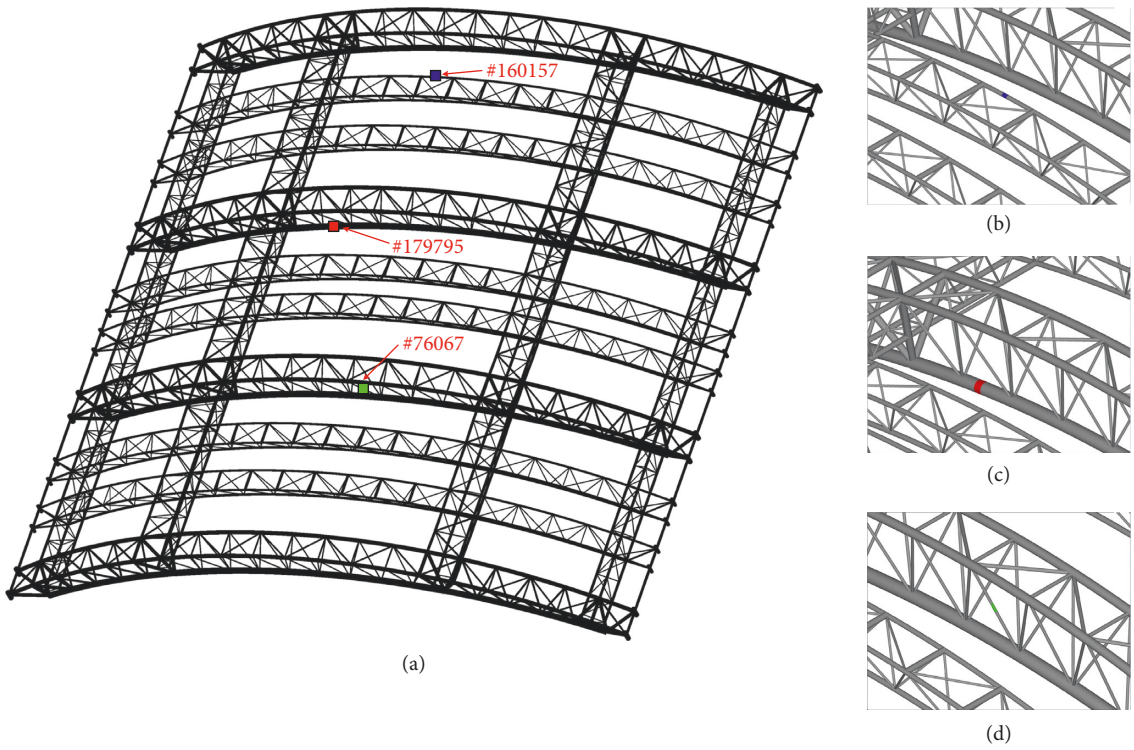

Figure 21: Layouts of element 160157, element 179795, and element 76067: (a) positions of the 3 chosen elements; (b) element 160157 (top chord); (c) element 179795(bottom chord); and (d) element 76067 (web member).

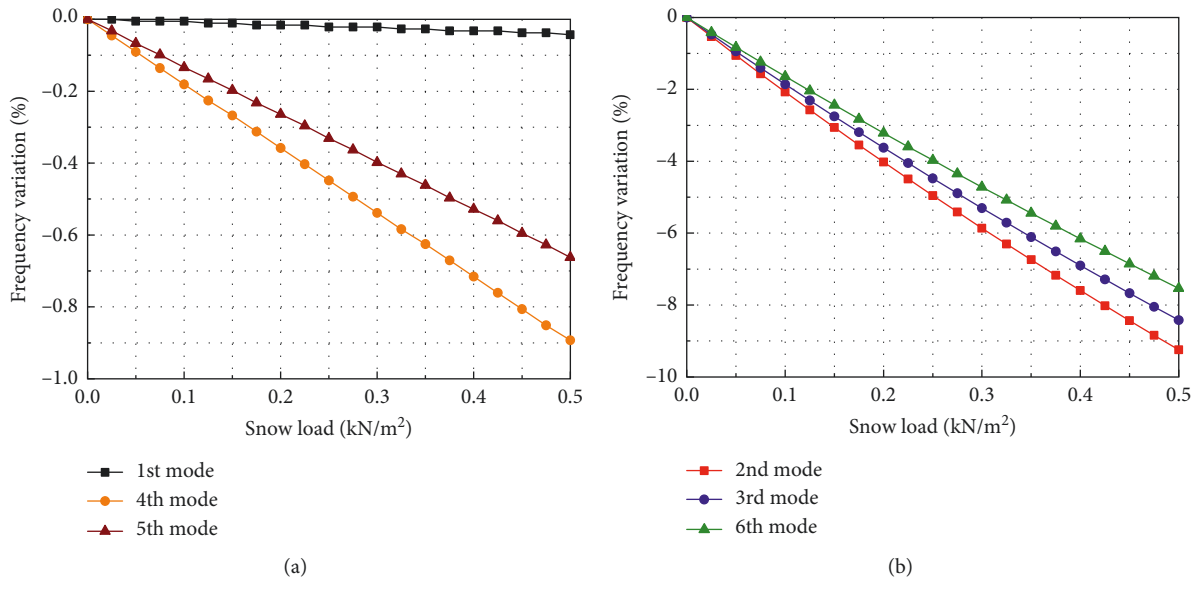

Figure 22: Frequency variations under uniformly distributed snow load: (a) the 1st, 4th, and 5th modes; and (b) the 2nd, 3rd, and 6th modes.

calculated as shown in Figures 23–25. According to the calculation results, the MAC values decrease at a growing rate, which suggests that variations in the mode shapes become increasingly obvious as the snow load increases. Corresponding to the changes of modal frequencies, changes in MAC values are more significant for the 2nd, 3rd, and 6th modes than the 1st, 4th, and 5th modes. This finding reveals that large variations in stiffness and mass in certain directions caused by snow load can cause significant variations in mode shapes as well. Additionally, as shown in Figures 24 and 25, changes in MAC values in the vertical and longitudinal directions with high stiffness are smaller than those in the transverse direction. This result indicates that variations of the mode shapes on different directions are closely related to the corresponding stiffness. Notably, the MAC value of the 6th mode shape exhibits the most significant changes in every

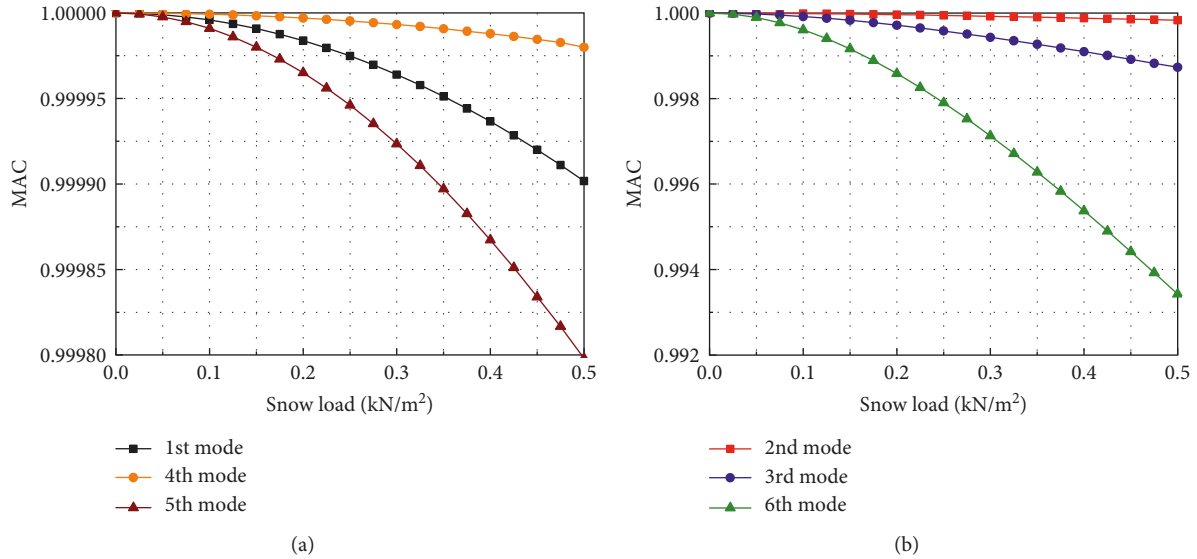

Figure 23: MAC values of the mode shapes on transverse direction under uniformly distributed snow load: (a) the 1st, 4th, and 5th modes and (b) the 2nd, 3rd, and 6th modes.

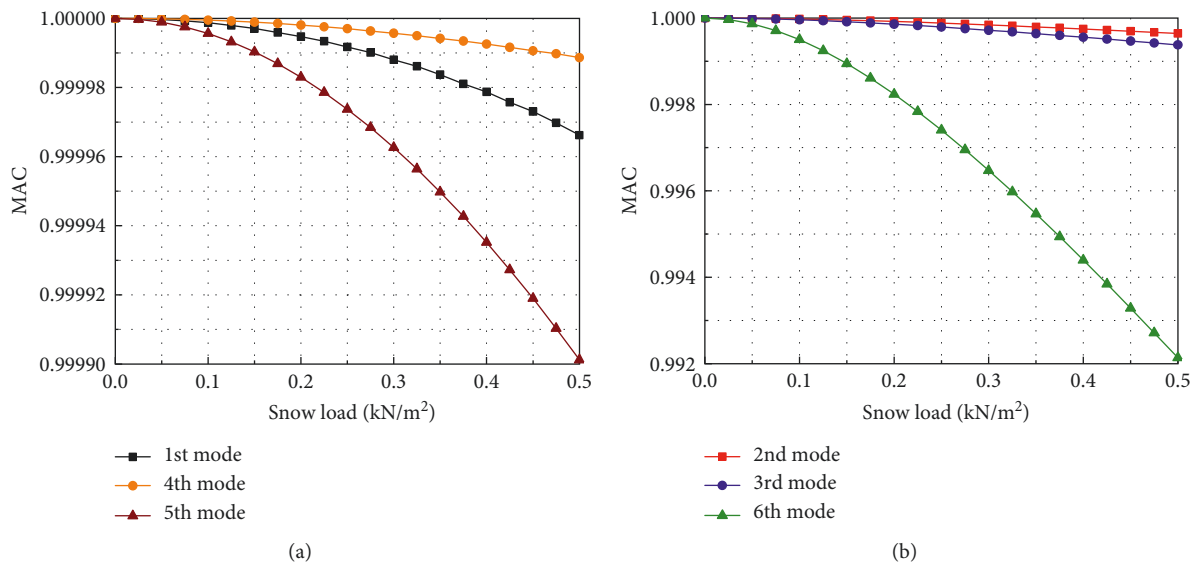

Figure 24: MAC values of the mode shapes on vertical direction under uniformly distributed snow load: (a) the 1st, 4th, and 5th modes and (b) the 2nd, 3rd, and 6th modes.

direction. This finding suggests that high modes with complicated mode shapes are more sensitive to the effects of the snow load. Additionally, the MAC values of the 2nd and 3rd modes exhibit similar variations due to their similar mode shapes. Overall, snow load affects modal parameters by changing the stiffness and mass matrices of the structure.

3.2.2. Analysis of a Nonuniform Snow Load Distribution Condition. As an external environmental load, the form and distribution of snowfall will change over time and become increasingly complex. The effects of wind, temperature, and freeze-thaw cycles can change, thereby influencing the distribution of the snow load. Consequently, this subsection focuses on the variations in modal parameters under the effects of a nonuniformly distributed snow load. For the steel structure roof of the Harbin Railway Station, the snowfall distribution will change over time. According to the reference of GB50009-2012 [18], the snow load on an arched roof can be calculated based on Figure 26. The snow pressure $\mu_{r,m}$ can be expressed as follows:

$$\mu_{r,m} = 0.2 + \frac{10f}{l}, \left(\mu_{r,m} \leq 2.0\right). \tag{13}$$

To investigate the variations in modal parameters under uniformly and nonuniformly distributed snow loads, the total mass of the snow load is held constant.

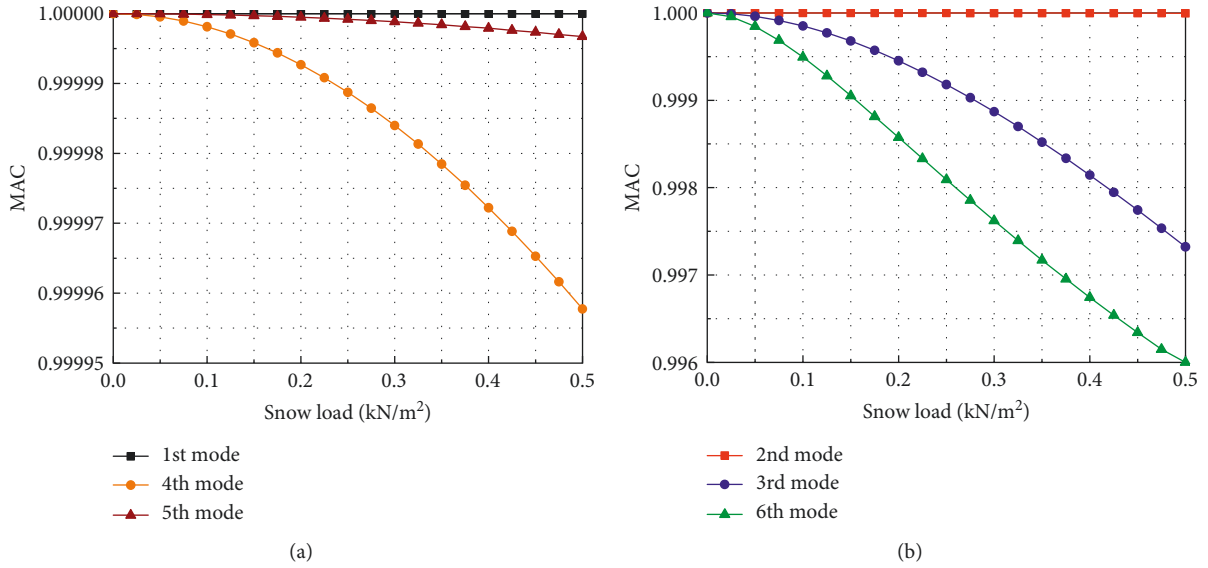

Figure 25: MAC values of the mode shapes on longitudinal direction under uniformly distributed snow load: (a) the 1st, 4th, and 5th modes and (b) the 2nd, 3rd, and 6th modes.

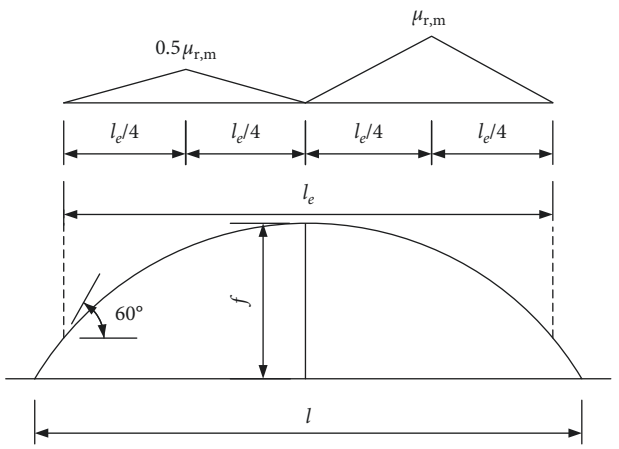

Figure 26: Distribution factor of snow pressure.

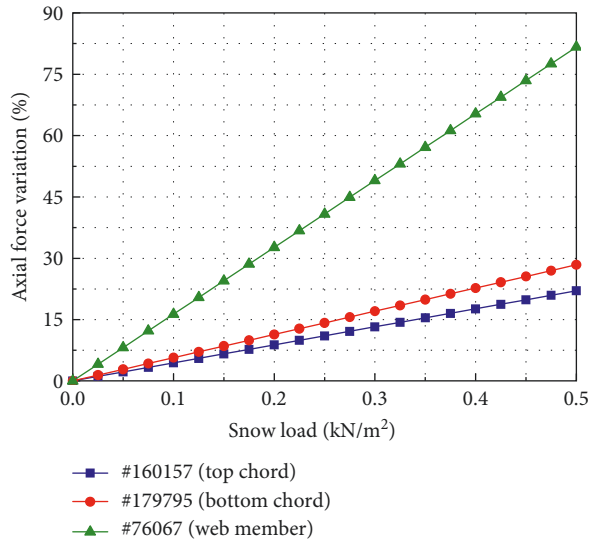

Figure 27: Axial force variations under nonuniformly distributed snow load.

Due to the nonuniform distribution of the snow load, changes in axial forces will have different results. According to Figure 27, despite the constant total mass of snow load, the axial forces on the typical elements of the top chord, bottom chord, and web members increase to various levels. Because the snow load is concentrated in the middle portion of the trusses, the load-bearing burden of the force members increases at the span center. Thus, the axial forces on the top chord and bottom chord changes in small increments at around 5%. Additionally, the axial forces on typical elements of the web members significantly increase by more than 65%. For the studied steel structure roof, the web members transfer the snow load from the top chord to bottom chord. Therefore, the local load-bearing variations associated with the top and bottom chords can drastically influence the corresponding web members. As a result, the responses of typical elements significantly increase.

Due to the close relationship between modal parameters and structural stiffness and mass matrices, changes in the distribution of the snow load can result in different variations. Figure 28 shows the variations in the first six modal frequencies for a nonuniformly distributed snow load. Compared above, the first six modal frequencies exhibit similar change trends under uniformly and nonuniformly distributed snow loads. It is noteworthy that because of the nonuniform distribution, the snow load on the exact center positions of the trusses is reduced. For the 1st, 4th, and 5th modes, the exact center position of the trusses includes high-amplitude positions according to Figures 13, 16, and 17. Consequently, the 1st, 4th, and 5th modes shown in Figure 28 exhibit at least two-fold reductions compared with those shown in Figure 22.

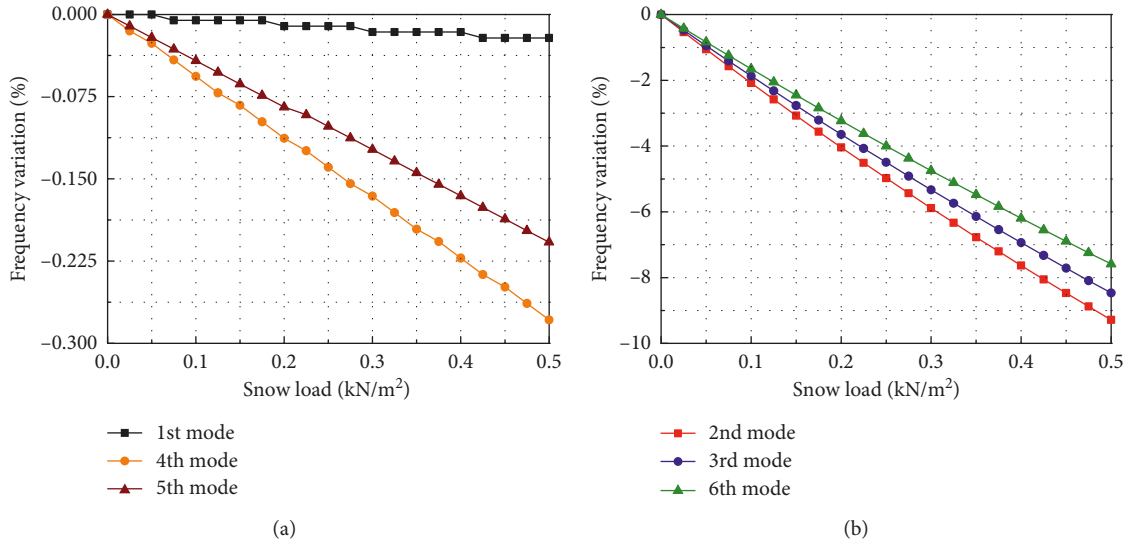

Figure 28: Frequency variations under nonuniformly distributed snow load: (a) the 1st, 4th, and 5th modes and (b) the 2nd, 3rd, and 6th modes.

In contrast, the nonuniformly distributed snow load has little effect on the transverse stiffness and mass matrices. As a result, the modal frequencies of the 2nd, 3rd, and 6th modes barely change. In summary, the different change regulations of modal frequencies under uniformly and nonuniformly distributed snow loads are the result of the internal changes on stiffness and mass matrices.

Compared to the modal frequencies, variations in the mode shapes are more closely related to internal differences in the structural stiffness and mass matrices. For the steel structure roof, variations of stiffness and mass matrices at different positions caused by the nonuniformly distributed snow load are more significant. As a result, the MAC values of different modes changed compared above. Figures 29–31 exhibit variations in MAC values in different directions for a nonuniformly distributed snow load. The variations in MAC values for the first six modes are mostly more obvious than those shown in Figures 23–25. However, some specific changing trends in MAC values should be noted. For the 1st mode, the center positions of the trusses are the locations with high amplitude. Due to the reduction of snow load on these positions, the stiffness and mass matrices show the least significant variation. Thus, the MAC value in the longitudinal direction exhibits little variation, as shown in Figure 31(a). However, due to the nonuniform distribution of the snow load, for the 1st mode, the variation quantities of stiffness and mass matrices increase in the transverse and vertical directions. Thus, MAC values in these two directions exhibit significant variations, as shown in Figures 29(a) and 30(a). Similarly, due to the same reason, the MAC values of the 4th and 5th modes display insignificant variations in the main vibration direction in Figure 30(a) and obvious variations in the other two directions, as shown in Figures 29(a) and 31(a). Additionally, for the MAC values of the 2nd, 3rd, and 6th modes, due to the relatively small variations of stiffness and mass matrices in the transverse direction for these modes, the variations are less notable than those of the 1st, 4th, and 5th modes. It is worth noting that the MAC value of the 6th mode in the vertical direction exhibits a unique trend, as shown in Figure 30(b). This finding may be due to the complex shape of the 6th mode, which could cause the MAC value to decrease in a unique manner under the nonuniformly distributed snow load. Moreover, this result indicates that high modes are more sensitive to the nonuniformly distributed snow load than low modes. In summary, the above phenomenon indicates that the effects of the nonuniformly distributed snow load on different mode shapes vary. Moreover, it again validates the close association between the variations of mode shapes and the changes of stiffness and mass matrices caused by nonuniformly distributed snow load.

Comparing the FEM results of static and dynamic responses, one aspect to notice is that change of modal parameters is far below the change of axial forces. As the snow load increases, the changes in the modal frequencies are mostly less than 10% and the decreases of MAC values are less than 0.01. It illustrates that modal parameters vary over a relatively small range under effects of snow load. Accordingly, for the SHM system of a structure, data collection of the dynamic responses needs to be quite accurate. In reality, due to advances in sensor technology, the response data collected by structural health monitoring system with high precision sensors are becoming more and more accurate. Studies on the modal parameters with small variation ranges can make the collected data better used. Furthermore, due to the small range of variation, identifications of actual changes and damages of the structure are likely to be covered by the variations of modal parameters caused by snow load effects. Consequently, it is of great importance to study the relationship between modal parameters and snow load to improve the accuracy and reliability of the SHM system.

4. Results of Structural Health Monitoring

4.1. Basic Information on Structural Health Monitoring Systems and Sensors. In the SHM systems of a spatial structure,

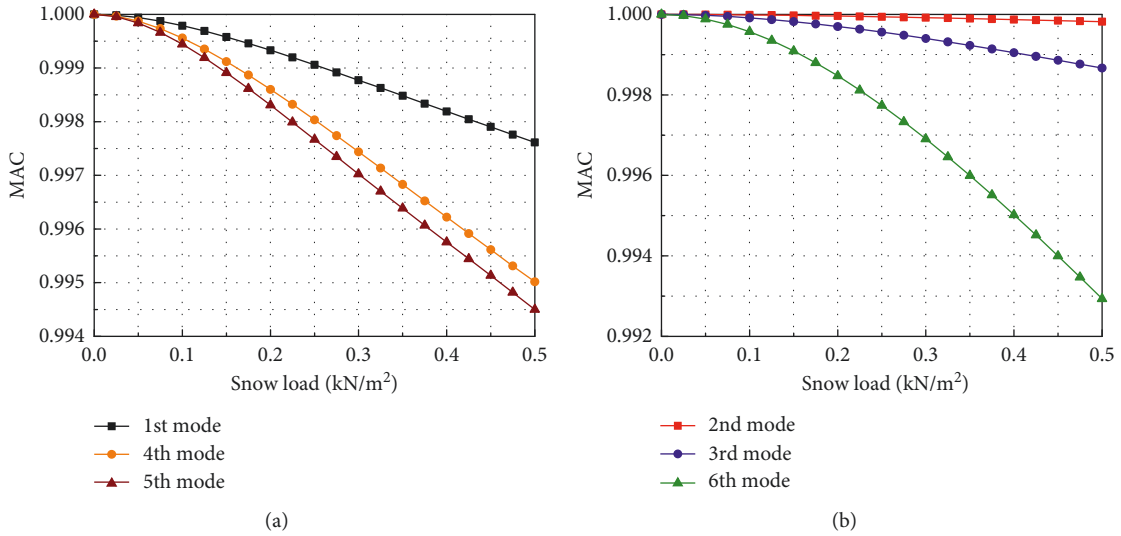

Figure 29: MAC values of the mode shapes on transverse direction under nonuniformly distributed snow load: (a) the 1st, 4th, and 5th modes and (b) the 2nd, 3rd, and 6th modes.

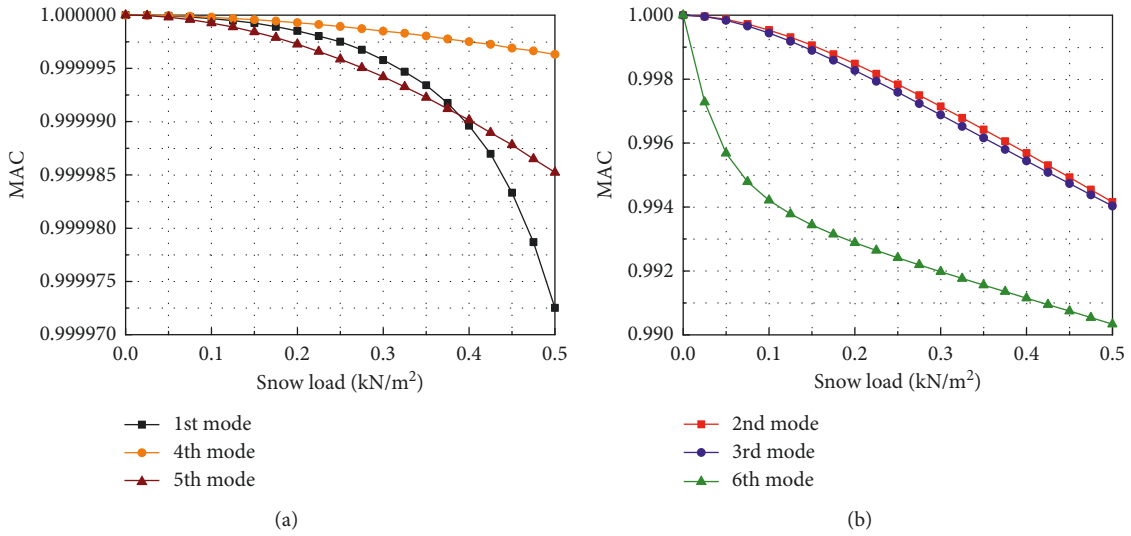

Figure 30: MAC values of the mode shapes on vertical direction under nonuniformly distributed snow load: (a) the 1st, 4th, and 5th modes and (b) the 2nd, 3rd, and 6th modes.

the most important and most widely used method for safety assessment, damage detection, and security prewarning is the identification of modal parameters based on actual structural behaviour data. However, the dynamic responses collected by the SHM system can also be affected by environmental factors. For the steel structure roof, effect of snowfall is the main factor to the structural responses. Accordingly, study of the snow load effects can reduce the impact to the identification of modal parameters and improve the accuracy of the SHM system.

For the steel structure roof of Harbin Railway Station, a SHM system was designed and implemented to collect and analyse the static and dynamic responses. The static responses can directly reflect the state of the structure. As is shown in Figures 32 and 33, optical fibre Bragg grating (OFBG) surface strain sensors were installed to collect the axial strains on typical top chords, bottom chords, and web members. 6 OFBG displacement sensors were installed to collect the horizontal displacements of the supports. 6 OFBG temperature sensors were installed to monitor the temperature changes. 5 static hydrostatic level gauges were installed to monitor the settlements occurring at the supports and typical positions of the structure. However, static response monitoring has limitations, and the positions without monitoring equipment are ignored. Therefore, it is necessary to collect dynamic responses for the identification of modal parameters. As a result, 5 3-D accelerometers were installed to collect the dynamic acceleration data on the typical positions. Table 2 and 3 show the properties of the sensors.

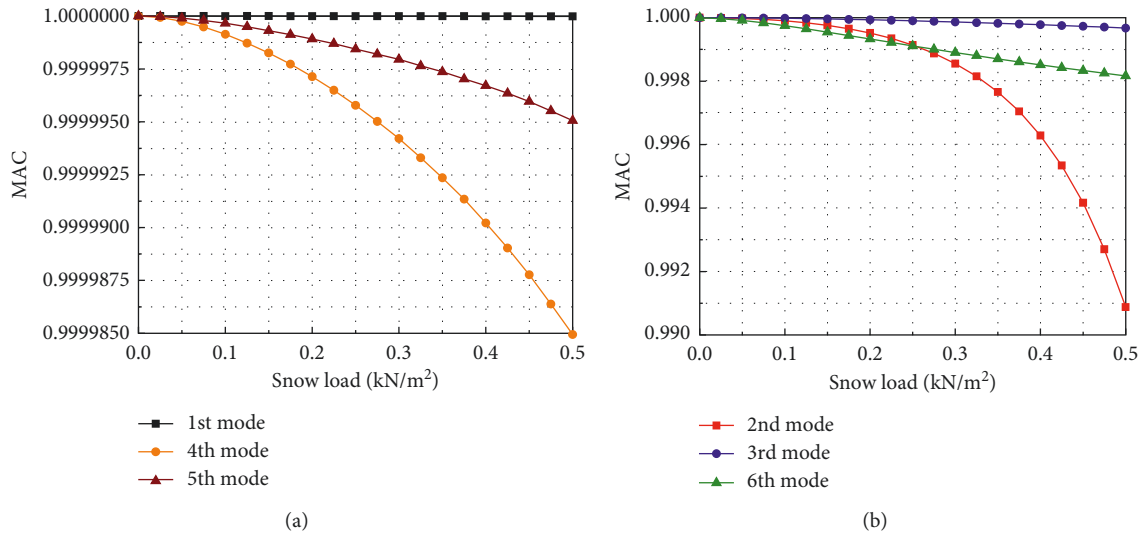

Figure 31: MAC values of the mode shapes on longitudinal direction under nonuniformly distributed snow load: (a) the 1st, 4th, and 5th modes and (b) the 2nd, 3rd, and 6th modes.

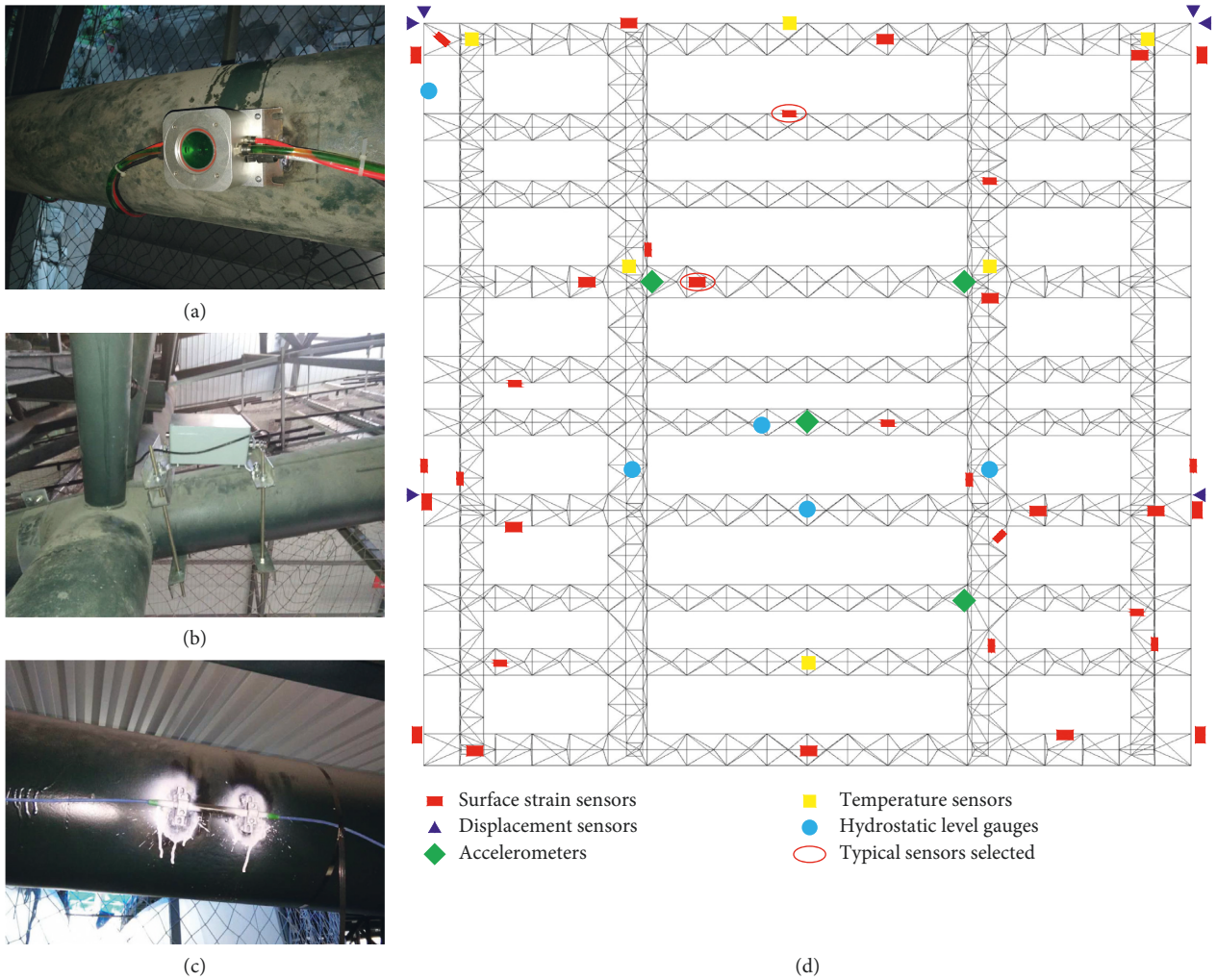

Figure 32: Layouts of hydrostatic level gauges, accelerometers, and OFBG sensors: (a) level gauge; (b) accelerometer; (c) OFBG sensor; and (d) layouts of the SHM system.

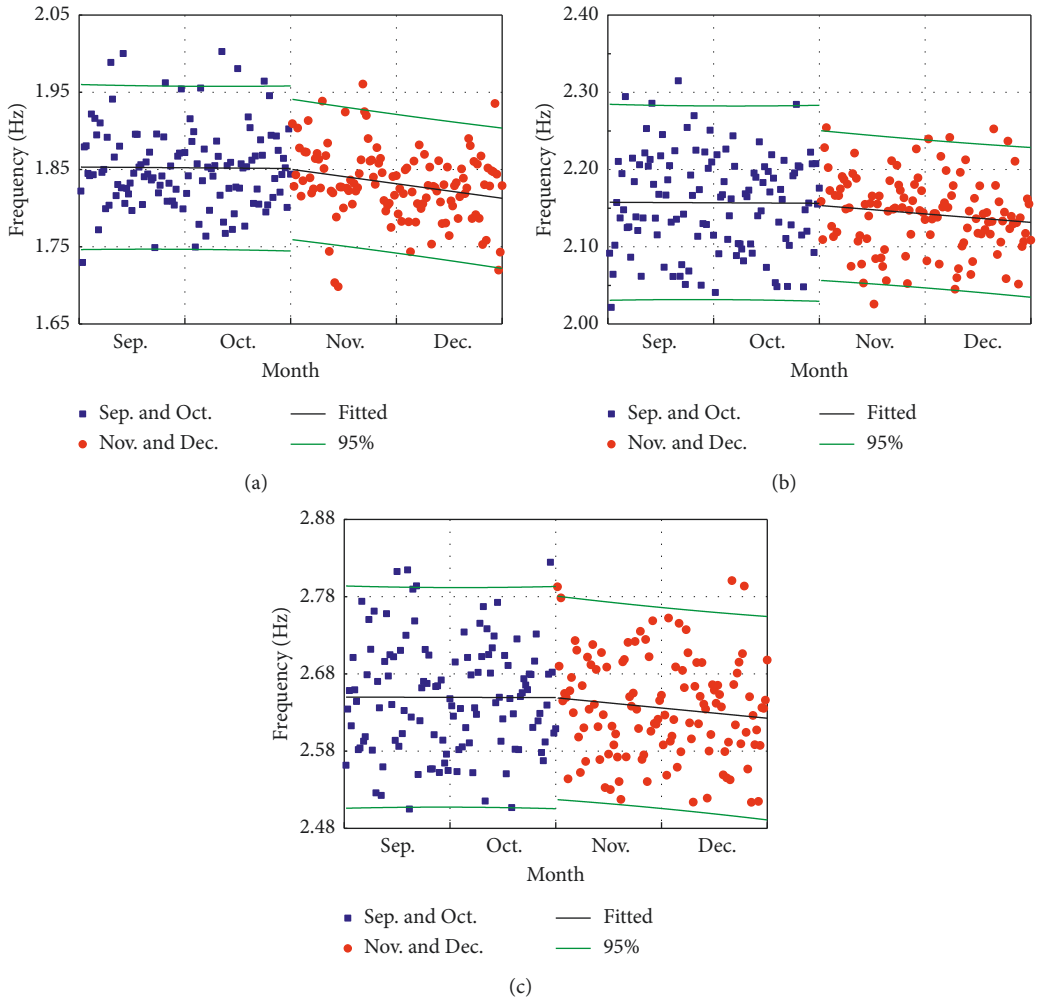

Figure 33: Frequency variation versus time: (a) the 1st modal frequency (longitudinal); (b) the 2nd modal frequency (transverse); and (c) the 4th modal frequency (vertical).

Table 2: Properties of surface strain sensors, temperature sensors, and displacement sensors.

Parameters	Surface strain sensors	Temperature sensors	Displacement sensors
Measurement range	$-1500\,\mu\varepsilon \sim +1000\,\mu\varepsilon$	−40°C~200°C	50 mm
Wavelength range	1510 nm~1590 nm	1510 nm~1590 nm	1510 nm~1590 nm
Precision	1‰ F.S.	0.08°C~0.1°C	1‰ F.S.
Resolution	0.5‰ F.S.	0.04°C	0.5‰ F.S.

Table 3: Properties of hydrostatic level gauges and accelerometers.

Parameters	Hydrostatic level gauges	Accelerometers
Measurement range	2 m	± 2.0 g
Operation temperature range	−30~80°C	−20°C~60°C
Precision	0.01% F.S	0~50 Hz
Resolution	0.003% F.S	<0.01 gal

4.2. Variations in Axial Strain. As noted above, the axial strains of certain members were monitored with OBFG surface strain sensors. The monitoring results of at 12:00 from 1 Sep. 2017 to 30 Dec. 2017 are displayed in Figure 34. According to Figure 32, the selected typical sensors locate at the same positions as the typical elements chosen in FEM results. Due to the small change in the ambient temperature, the major environmental influence on the structure is snowfall. Thus, the monitoring results can be divided into two parts according to the time of the first snowfall. According to the weather in Harbin, the first snowfall occurred on 9 Nov. 2017. According to Figure 34, the axial strain responses at typical positions on the top chord and bottom chord exhibited insignificant change in Sep. and Oct. In the following Nov. and Dec., the axial strain increased, especially on the day after a snowfall event, as a result of snow accumulation on the roof. Correspondingly to the FEM results discussed above, snow load can directly increase the load-bearing burden of the structure. Additionally, the

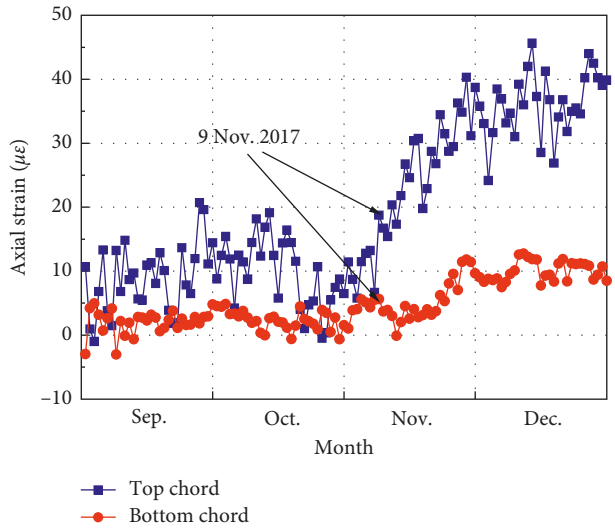

Figure 34: Axial strain variation.

second moment of area of the bottom chord is larger than the top chord does. As a result, the monitoring result of the top chord changes more significantly with larger fluctuations.

4.3. Modal Identification Method and Modal Parameters. Modal identification methods have been designed and proposed to improve the accuracy, resolution, and reliability of estimating modal parameters. Due to the low signal-to-noise ratio of the measured acceleration signal, modal identification methods with high resolution, high accuracy, and strong noise-resistance ability should be selected and used [20]. For instance, the Eigensystem Realization Algorithm (ERA) combined with the Natural Excitation Technique (NExT) [21–23] is a common modal identification method that has been widely applied for the identification of modal parameters.

It is worth noting that the variations of modal parameters are closely related to the frequency characteristics of the loading. For instance, fluid-structure coupling effects caused by wind and explosion load with different ranges of frequencies can change the modal parameters of the structure in different forms and degrees. However, no kinds of load with specific ranges of frequency characteristics generated during the process of collecting structural response data. Therefore, the dynamic response of the steel structure roof can be considered as vibration caused by natural excitation. As a result, in this study, modal parameters of the steel structure roof were identified through NExT + ERA in the temporal domain using acceleration response data collected by the 3-D accelerometers.

According to the previous FEM-based analyses, the modal frequencies are quite close among the first 60 orders. Moreover, the higher mode shapes become more and more complicated as well. Consequently, the identification results of higher orders have lower reliability and are difficult to distinguish. Therefore, due to their relatively simple and stable mode shapes, the 1st, 2nd, and 4th modal parameters were identified. The 3rd mode was skipped because it has a mode shape similar to that of the 2nd mode. In the process of Fourier transformation, the range of cut-off frequency was set from 1 Hz to 3 Hz to eliminate the interference of high and low orders of modal frequencies.

For the purpose of comparing to the calculation results shown above, the acceleration responses at 12:00 on 13 Sep. 2017 were selected, i.e., the impact of snowfall has not yet occurred. According to the identification results, the 1st, 2nd, and 4th modal frequencies were 1.8463 Hz, 2.1573 Hz, and 2.6489 Hz, respectively. The results agree well with the calculated modal frequencies and the differences are less than 2%. Additionally, the corresponding identified mode shapes are shown in Figure 35 (mode shape coefficients are magnified for clarity). The identified 1st mode shape shows a significant structural deformation on longitudinal direction, which is consistent with the calculated result shown in Figure 13. Changes in the center of the transverse trusses are especially obvious. Additionally, Figure 35(b) shows the same kind of deformation trend on the transverse direction as Figure 14 does. The relative position of each truss is gradually offset in the transverse direction. For the 4th order, the identified mode shape shows a conspicuous form of vertical vibration, which is the same as the calculation result in Figure 16. The displacements of the 1st and 10th trusses in the vertical direction are significantly different. Overall, the identified 1st, 2nd, and 3rd modal frequencies and their corresponding mode shapes all agree well with the calculated results of FEM analysis. The accuracy of these two research methods is proved through the contrast results.

4.4. Variations in Natural Structural Frequencies. As discussed above, effects of snowfall occurred in Nov. and Dec. 2017 changed the axial strains of the steel structure roof. Correspondingly, the dynamic responses were altered by snow load as well. The acceleration records (collected by the 3-D accelerometers from 1 Sep. 2017 to 31 Nov. 2017) were identified using the NExT + ERA method to obtain the relationship between the modal frequency and snow load. Figure 33 shows the identification results of the 1st, 2nd, and 4th modal frequencies. For the three orders, since no

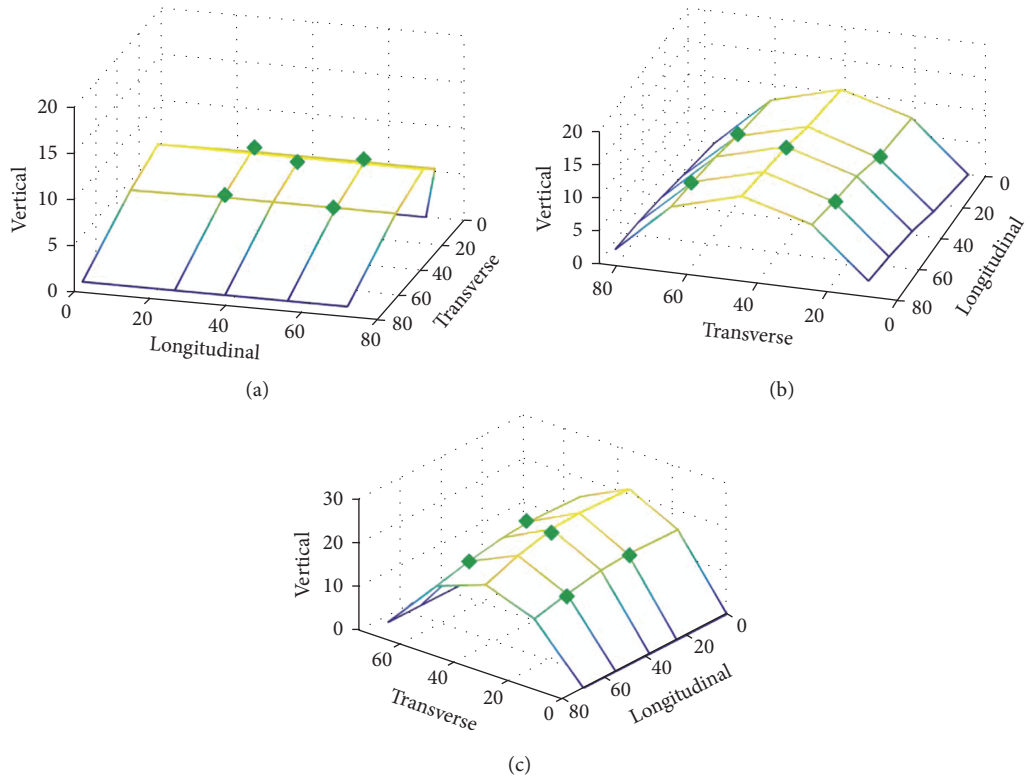

Figure 35: Mode shapes identified using NExT + ERA from 12:00:00, 13 Sep. 2017 to 12:30:00, 13 Sep., 2017: (a) the 1st mode shape (longitudinal); (b) the 2nd mode shape (transverse); and (c) the 4th mode shape (vertical).

snowfall occurred, the fitting results of the identified frequencies remain approximately constant in Sep. and Oct at around 1.8520 Hz, 2.1570 Hz, and 2.6496 Hz, respectively. As can be seen, the fitting results are in good agreements with the calculated FEM results shown above. Similarly, the identified modal frequencies decrease as snow load increases. After entering Nov., snowfall accumulated on the structure and the identified frequencies show continuous downward trends. Specifically, the decreased responses in Dec. were particularly obvious. The fitting results gradually decrease to 1.8159 Hz, 2.1274 Hz, and 2.6275 Hz. The reductions are less than 2%, which are basically kept at the same order of magnitude to the FEM results. Overall, the calculated modal frequencies and their fitting results are in good agreements with the analysis results through FEM. As is discussed, the accuracy of these two research methods is once again been proved. Additionally, one noticeable and similar phenomenon is that despite these decreases, the distributions of the modal frequencies measured from Nov. to Dec. almost cover the same range as the results measured from Sep. to Oct. It is illustrated that the identification results vary over a relatively small range under effects of snow load, which is the same as the FEM result does. In summary, it is concluded that the research methods applied in this study are feasible and credible for the investigation of snow load effects on structural modal parameters.

4.5. Variations in Structural Damping Ratios. In the identification, the proportional viscous damping was assumed to be existence and the damping ratios of the steel structure roof extracted were through NExT + ERA. Figure 36 shows the damping ratios of the 1st, 2nd, and 4th orders. Similarly, without effects of snow load, the fitting results of the damping ratios barely change from Sep. to Oct. at around 0.0445, 0.0469, and 0.0459, respectively. Whereas a negative relationship could be observed from Nov. to Dec as the snowfall occurred and the damping ratios drop to 0.0331, 0.0382 and 0.0375. It is indicated that the damping ratios decrease along with the increasing snow load as well. Furthermore, it is worth noting that the identified damping ratios decrease more obviously than the case for frequencies and the reductions are about 20%. This phenomenon illustrates that the damping ratio is more sensitive to the effects of snow load than the modal frequency does.

5. Conclusions

This paper investigates the effects of snow load to the modal parameters of spatial structures based on a SHM system of the steel structure roof of Harbin Railway Station. The following conclusions were drawn from this study:

(1) According to the theoretical analysis of a single-span simply supported beam, the modal frequencies decrease with increasing snow load and the decreasing rate gradually diminishes. The diversities of change regulations among different modes are closely related to the distributions of the snow loads. When the snow loads are centrally distributed on the high-amplitude

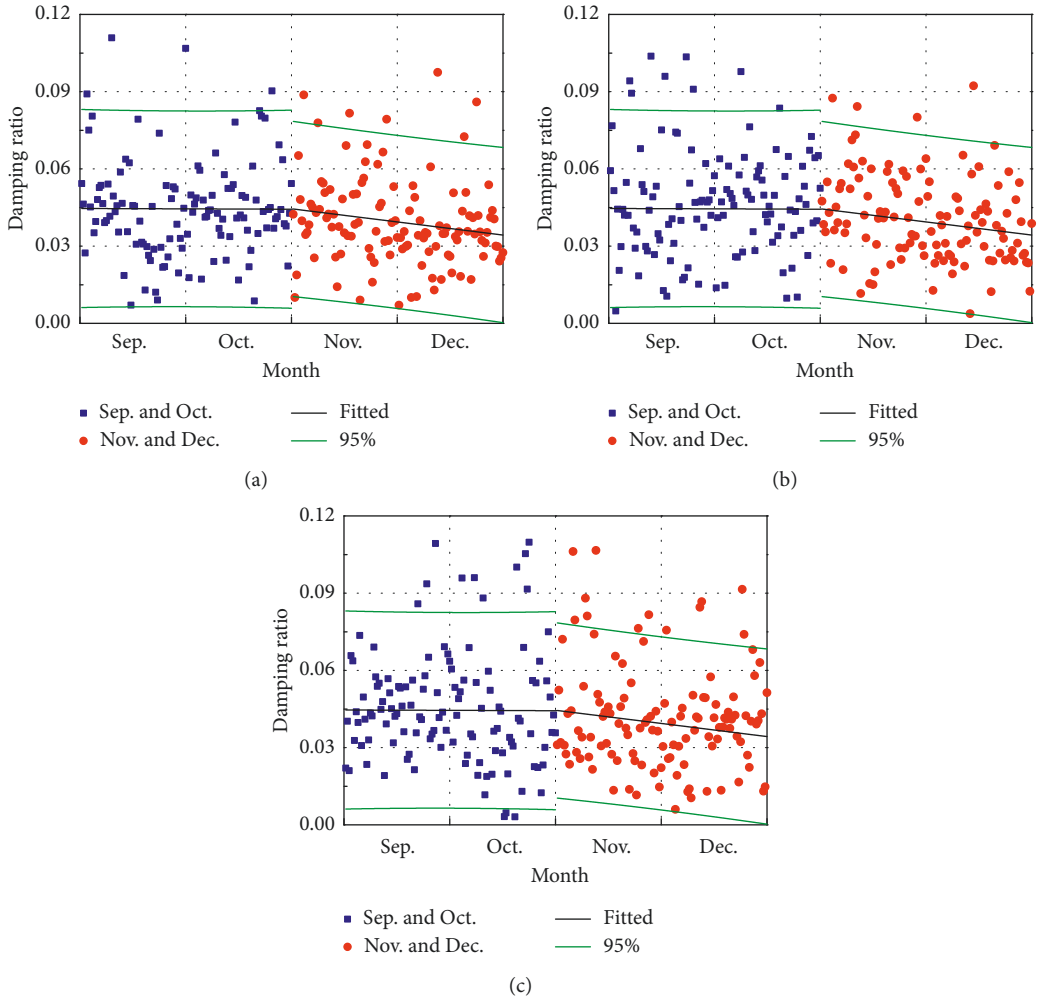

Figure 36: Damping ratio variation versus time: (a) the 1st mode damping ratio (longitudinal); (b) the 2nd mode damping ratio (transverse); and (c) the 4th mode damping ratio (vertical).

positions of certain modes, changes of the modal frequencies and mode shapes were significant.

(2) Variations of mode shapes are correlated to internal differences in structural stiffness and mass matrices caused by snow loads. Theoretical analysis showed that when the snow load was considered as a density change of the structure and no internal differences in stiffness or mass existed, the mode shapes barely change. Conversely, significant variations of mode shapes can be found when the snow loads were nonuniformly distributed.

(3) Both the theoretical analysis and the FEM results of the steel structure roof exhibit the same change regulations of modal frequencies under effects of snow load. The calculated MAC values decrease as the snow loads increase, which revealed the increasingly significant change of the mode shapes. According to the FEM results, variations of modal parameters among different modes are largely determined by the actual form of the mode shapes. Changes of stiffness and mass matrices caused by snow loads are different for each mode and the modal parameters show various changes.

(4) By comparison, both the modal frequency and mode shape variations of the steel structure roof exhibit close relationships with the distribution of the snow load. Due to the different distributions, snow loads bring dissimilar effects despite the unchanged total mass. Correspondingly, the mode shapes changed with varying degrees and several particular changes were observed for certain modes. Additionally, high modes with complicated mode shapes were more sensitive to the effects of the snow load.

(5) Based on the identification and analysis of the SHM data, it is concluded that snowfall-induced variations of stiffness and mass matrices cause the changes of modal parameters. The identified results of modal frequency and mode shape basically agree well with the analysis results, which proved the accuracy of the theoretical analysis and the FEM calculation. Both the identified and FEM results show less obvious variations on the modal parameters of the structure

than on the internal forces. These results indicate that modal parameters vary over a relatively small range under effects of snow loads.

(6) The identified damping ratios decrease along with the increasing snow loads. Compared to the identified results of modal frequencies, the damping ratios are exhibited to be more sensitive to the effects of snow loads.

(7) The investigation methods used in this research are proved to be feasible and credible for the investigation of snow load effects. In addition, the actual distribution of snow loads on the steel structure roof from 1 Nov. to 31 Dec. 2017 was not measured due to the high difficulty and the huge amount of work. In reality, the actual distribution of snow load could be very helpful to further improve the accuracy of FEM results and have better fidelity to the identified results. And more quantitative conclusions could be derived, accordingly.

Data Availability

The data used to support the findings of this study are available from the corresponding author upon request.

Conflicts of Interest

The authors declare that there are no conflicts of interest regarding the publication of this article.

Acknowledgments

The research has been financially supported by the China Railway Construction Engineering Group (Grant no. KY10200170035). Additionally, the authors gratefully acknowledge the financial support provided by the Natural Science Foundation of Heilongjiang Province under grant no. QC2016057.

References

[1] S. D. Glaser, H. Li, M. L. Wang, J. Ou, and J. Lynch, "Sensor technology innovation for the advancement of structural health monitoring: a strategic program of US-China research for the next decade," *Smart Structures and Systems*, vol. 3, no. 2, pp. 221–244, 2007.

[2] M. Majowiecki, "Snow and wind experimental analysis in the design of long-span sub-horizontal structures," *Journal of Wind Engineering and Industrial Aerodynamics*, vol. 74-76, pp. 795–807, 1998.

[3] B. Ellingwood and M. O'Rourke, "Probabilistic models of snow loads on structures," *Structural Safety*, vol. 2, no. 4, pp. 291–299, 1985.

[4] M. O'Rourke and C. De Angelis, "Snow drifts at windward roof steps," *Journal of Structural Engineering*, vol. 128, no. 10, pp. 1330–1336, 2002.

[5] V. Meløysund, K. R. Lisø, H. O. Hygen, K. V. Høiseth, and B. Leira, "Effects of wind exposure on roof snow loads," *Building and Environment*, vol. 42, no. 10, pp. 3726–3736, 2007.

[6] R. H. Plaut, J. K. S. Goh, M. Kigudde, and D. C. Hammerand, "Shell analysis of an inflatable arch subjected to snow and wind loading," *International Journal of Solids and Structures*, vol. 37, no. 31, pp. 4275–4288, 2000.

[7] M. Holicky and M. Sykora, "Safety of lightweight steel roofs exposed to snow load," in *Proceedings of 5th European Conference on Steel and Composite Structures, Research-Practice-New Materials*, Graz, Austria, September 2008.

[8] M. Lazzari, M. Majowiecki, R. V. Vitaliani, and A. V. Saetta, "Nonlinear F.E. analysis of montreal olympic stadium roof under natural loading conditions," *Engineering Structures*, vol. 31, no. 1, pp. 16–31, 2009.

[9] A. Flaga, G. Kimbar, and P. Matys, "A new approach to wind tunnel similarity criteria for snow load prediction with an exemplary application of football stadium roof," in *Proceedings of European and African Conference on Wind Engineering*, Florence, Italy, July 2009.

[10] J. J. Del Coz Díaz, F. P. Álvarez Rabanal, P. J. García Nieto, J. Roces-García, and A. Alonso-Estébanez, "Nonlinear buckling and failure analysis of a self-weighted metallic roof with and without skylights by FEM," *Engineering Failure Analysis*, vol. 26, pp. 65–80, 2012.

[11] X. Sun, R. He, and Y. Wu, "Numerical simulation of snowdrift on a membrane roof and the mechanical performance under snow loads," *Cold Regions Science and Technology*, vol. 150, pp. 15–24.

[12] J. R. Hutchinson and S. D. Zillmer, "On the transverse vibration of beams of rectangular cross-section," *Journal of Applied Mechanic*, vol. 53, no. 1, pp. 39–44, 1986.

[13] S. M. Han, H. Benaroya, and T. Wei, "Dynamics of transversely vibrating beams using four engineering theories," *Journal of Sound and Vibration*, vol. 225, no. 5, pp. 935–988, 1999.

[14] B. Qian, "Research on numerical computation of natural frequency of transverse vibration for simply supported beam of non-uniform," *Applied Mechanics and Materials*, vol. 71–78, pp. 3316–3319, 2011.

[15] C. H. Chang, "Free vibration of a simply supported beam carrying a rigid mass at the middle," *Journal of Sound and Vibration*, vol. 237, no. 4, pp. 733–744, 2000.

[16] E. Özkaya, "Non-linear transverse vibrations of a simply supported beam carrying concentrated masses," *Journal of Sound and Vibration*, vol. 257, no. 3, pp. 413–424, 2002.

[17] S. J. Zhu, Y. F. Zheng, and Y.M. Fu, "Analysis of non-linear dynamics of a two-degree-of-freedom vibration system with non-linear damping and non-linear spring," *Journal of Sound and Vibration*, vol. 271, no. 1-2, pp. 15–24, 2004.

[18] China Architecture & Building Press, *Load Code for the Design of Building Structures*, China Architecture & Building Press, Beijing, China, 2012.

[19] M. Pastor, M. Binda, and T. Harčarik, "Modal assurance criterion," *Procedia Engineering*, vol. 48, pp. 543–548, 2012.

[20] J. Juang and R. S. Pappa, "Effects of noise on modal parameters identified by the eigensystem realization algorithm," *Journal of Guidance, Control, and Dynamics*, vol. 9, no. 3, pp. 294–303, 1986.

[21] M. Chang and S. N. Pakzad, "Modified natural excitation technique for stochastic modal identification," *Journal of Structural Engineering*, vol. 139, no. 10, pp. 1753–1762, 2013.

[22] J. M. Caicedo, S. J. Dyke, and E. A. Johnson, "Natural excitation technique and eigensystem realization algorithm for

phase I of the IASC-ASCE benchmark problem: simulated data," *Journal of Engineering Mechanics*, vol. 130, no. 1, pp. 49–60, 2004.

[23] D. Chiang and C. Lin, "Identification of modal parameters from ambient vibration data using eigensystem realization algorithm with correlation technique," *Journal of Mechanical Science and Technology*, vol. 24, no. 12, pp. 2377–2382, 2010.